University of Crete, Department of Physics

FO.R.T.H., Institute of Electronic Structure and Lasers

Bachelor Thesis

# Measurement of M1 and E2 components of the atomic iodine transition at 1315 nm using cavity-enhanced absorption spectroscopy

Name: Zoi Sargianni

Supervisor: Prof. T. Peter Rakitzis

ΠΑΝΕΠΙΣΤΗΜΙΟ ΚΡΗΤΗΣ
UNIVERSITY OF CRETE

# Contents

# Table of figures

# Abstract

The aim of this thesis is the study of the $5^2P_{3/2} \rightarrow 5^2P_{1/2}$ magnetic dipole (M1) transition of atomic iodine, $^{127}\mathrm{I}$, at $1315\mathrm{nm}$ using an optical-cavity-enhanced absorption scheme. Combining high atomic iodine densities, produced via high-power photodissociation of molecular iodine at 532nm, and long interaction pathlengths, due to the high-finesse optical cavity setup, we produced high atomic iodine *column* densities, which enabled the measurement of the electric quadrupole (E2) component of the transition of interest. These quadrupole component measurements performed in our lab are the only such measurements to the best of our knowledge. The dimensionless ratio of E2 to M1 matrix elements was found to be $\chi = E2/M1 = [\mathbf{0.085} \pm \mathbf{0.004}]$, with $M1 = 1.15\mu_B = 0.0042e\alpha_B$.

Regarding the structure of this thesis, in the first part we describe the required theory: gaussian beams, optical cavities, then the theory of atomic transitions, both from the side of the effect of matter on light (Maxwell equations, atomic medium polarization, index of refraction), as well as from the side of the effect of light on matter (transition rates, absorption and stimulated emission of radiation, cross-sections, multipole expansion of the electric field and allowed/forbidden transitions, and selection rules). Then, the specific theory of the relevant M1 transition of iodine and a brief discussion of the photodissociation process of molecular iodine into atomic are given. In the second part of the thesis, we present the experimental scheme, we describe the measurement process, and finish with the analysis of the results and our conclusions.

# Theory

## Gaussian beams

By the term gaussian beam we mean a mathematical model that describes the electric field distribution of propagating light. This is achieved by an approximate analytical solution to the wave equation. The intensity distribution in a plane perpendicular to the propagation direction of most optical beams propagating in free space is almost pure TEM (transverse electric and magnetic) modes. The Gaussian beams diverge with the lowest possible rate due to diffraction.

The lowest-order $\mathrm{TEM}_{0,0}$ mode is given by the following equation, where $E(x,y,z)$ is the electric field intensity at Cartesian coordinates $(x,y,z)$:

$$E(x,y,z) = E_0 \underbrace{\left\{\frac{w_0}{w(z)}\exp\left[-\frac{r^2}{w^2(z)}\right]\right\}}_{\text{Amplitude factor}} \times \underbrace{\exp\left\{-j\left[kz - \tan^{-1}\left(\frac{z}{z_R}\right)\right]\right\}}_{\text{Longitudinal phase}} \times \underbrace{\exp\left[-j\frac{kr^2}{2R(z)}\right]}_{\text{Radial phase}} \quad (1)$$

where $r = \sqrt{x^2 + y^2}$ and $\boldsymbol{z}$ the propagation direction.

To abbreviate the various terms above, the quantities below are defined. The beam width as a function of propagation distance, $z$, as depicted in *Figure 1*, is:

$$w^2(z) = w_0^2\left[1 + \left(\frac{\lambda_0 z}{\pi n w_0^2}\right)^2\right] \quad (2)$$

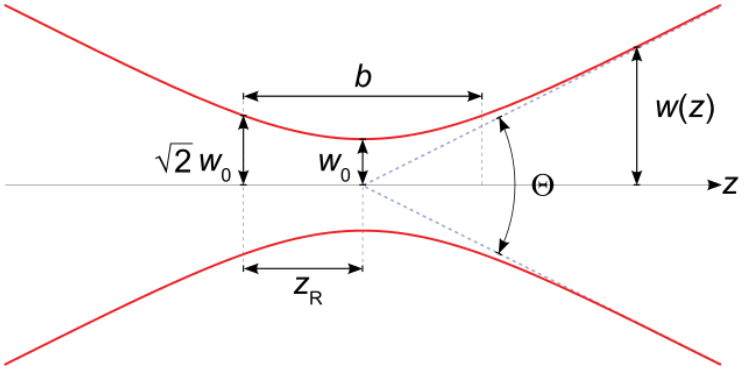


*Figure 1: Gaussian beam width w(z)*
*from www.wikiwand.com*

The radius of curvature of the phase front, $R(z)$, is:

$$R(z) = z\left[1 + \left(\frac{z_R}{z}\right)^2\right] \tag{3}$$

where $z_R$ is the characteristic length parameter of the Gaussian beam also called as *Rayleigh distance* or *Rayleigh range*:

$$z_R = \frac{\pi n w_0^2}{\lambda_0} \tag{4}$$

and $w_o$ is the minimum spot size:

$$w_0^2 = \frac{2z_0}{k} = \frac{\lambda_0 z_R}{n\pi} \tag{5}$$

$\lambda_0$ is the free-space wavelength, n is the index of refraction, $k = \frac{2\pi n}{\lambda_0} = \frac{\omega n}{c}$ is the wavenumber, r is the radial coordinate and $\omega$ is the angular frequency.

## Optical Cavity

An optical cavity is an arrangement of highly reflective mirrors. There are two kinds of cavities; running wave cavities, where light propagates in one direction on a closed path inside the cavity and standing wave cavities where light goes back and forth on a specific path. For certain *resonant* frequencies, light inside the cavity interferes constructively with the incoming light, and, as a result, energy build-up occurs inside the cavity. That is to say, optical cavities only support certain resonant frequencies of light, i.e., they have a discrete spectrum, which depends on the length of the cavity, and the index of refraction of the medium inside it. One can use various mirror arrangements to form optical cavities (two-mirror, three-mirror, four-mirror etc.); we use a bow-tie-shaped type, which is a four-mirror cavity resembling a bowtie, as depicted in *Figure 2 (a)*.

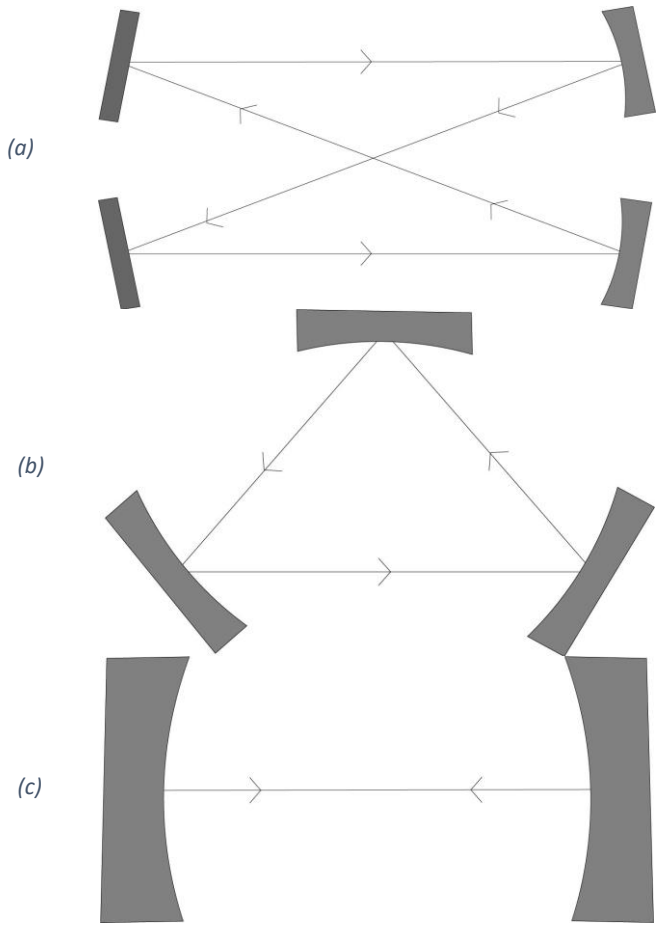


*Figure 2: Cavity configurations: (a) Standard bow-tie cavity, (b)three-mirror cavity, (c) two-mirror cavity*

When light propagates inside an optical cavity, only certain patterns of light (i.e., beam intensity distributions), called resonant modes, are allowed. A cavity mode is defined as a field distribution that reproduces itself in relative phase after a round trip through the system. Using spherical (and flat) mirrors for the implementation of optical cavities, symmetry considerations lead to the transverse light patterns to take the form of the, so called, *Transverse Electric Modes*, $\text{TEM}_{nm}$. These are the spatial distribution of the electric field's amplitude on a plane perpendicular to the axis of light propagation. *Hermite-Gaussian modes* are approximate solutions of the wave equation for the paraxial approximation. If we assume that the propagation axis is in the z-direction in a Cartesian coordinate system, then the shape of the electric field's amplitude profile is described by the equation below:

$$E_{nm}(x,y,z) = E_0 \frac{w_0}{w(z)} \cdot H_n\left(\sqrt{2}\frac{x}{w(z)}\right) \cdot H_m\left(\sqrt{2}\frac{y}{w(z)}\right) \cdot \exp\left(-\frac{x^2+y^2}{w(z)^2}\right) \cdot \exp\left(-i\left[kz - (1+n+m)\arctan\frac{z}{z_R} + \frac{k(x^2+y^2)}{2R(z)}\right]\right) \quad (6)$$

where $H_n(x)$ (or $H_m(y)$) is the Hermite polynomial with the non-negative integer index *n* (or *m*) that determines the order, i.e., the shape, of the profile in the x-direction (or y-direction). Specifically, these indices define the number of nodes of zero intensity in each direction. The Hermite polynomials are given by $H_n(x) = (-1)^n e^{x^2} \frac{d^n}{dx^n} e^{-x^2}$. The intensity profiles of the lowest-order Hermite-Gaussian modes are represented in *Figure 3*.

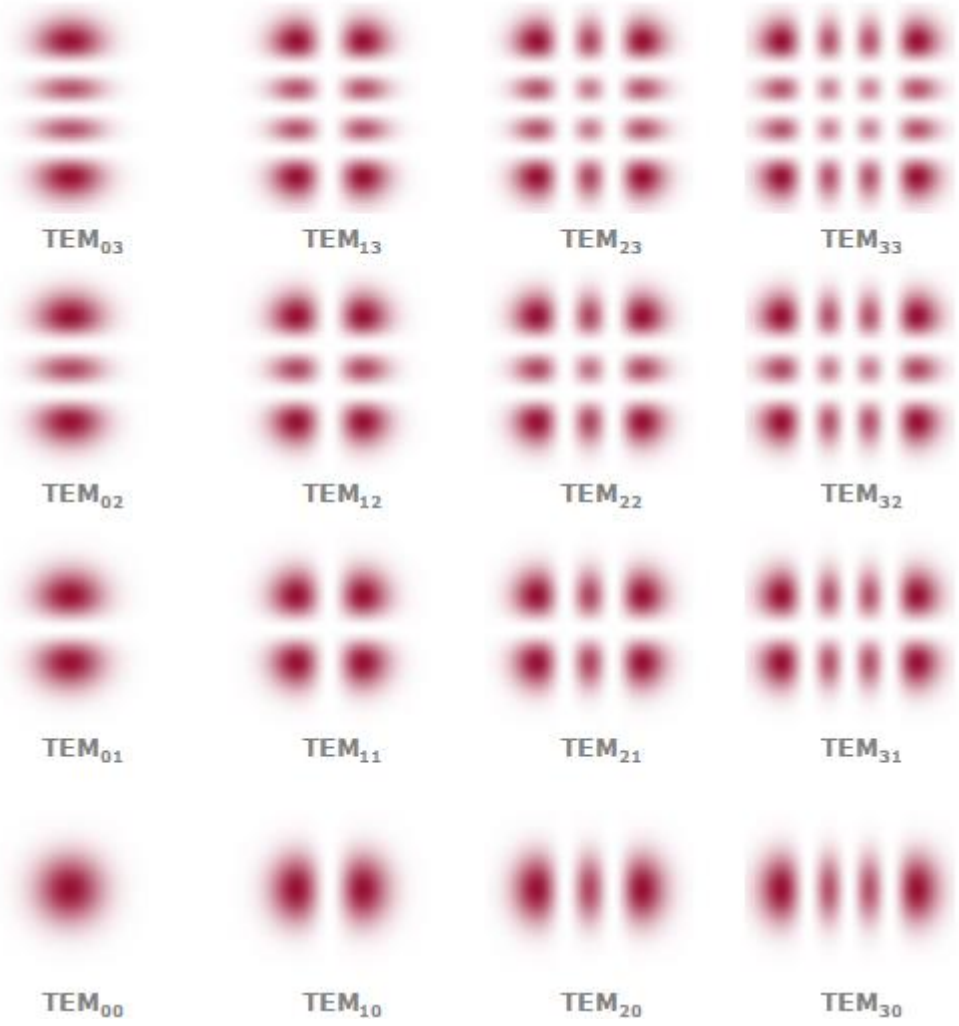


*Figure 3: Intensity profiles of the lowest-order Hermite–Gaussian modes from www.rp-photonics.com*

Let's look at a two-mirror cavity, like the one in *Figure 4* (or in *Figure 2 (c)*), with mirror reflectivities $M_1$ and $M_2$. We consider all waves, incident on the cavity from the left, inside the cavity, or transmitted through it to the right to be plane waves.

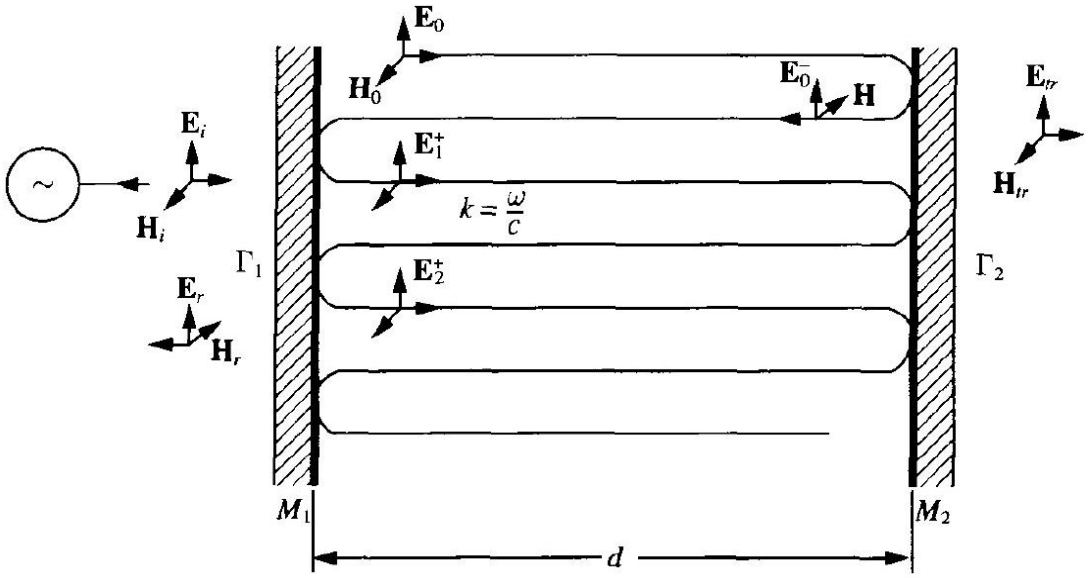


*Figure 4: Optical cavity. Image from Verdeyen – Laser Electronics*

Let's follow a wave that bounces back and forth between the two mirrors. As the initial field, $E_0$, just to the right of $M_1$, propagates to $M_2$ and back its amplitude changes by the factor $\Gamma_1 \cdot \Gamma_2$ and accumulates the phase term $\exp(-ik2d)$, where $2d$ is the round trip length. Thus, it generates the field $E_1^+$ that experiences the same changes as $E_0$, and $E_1^+$ generates $E_2^+$, and so on. The fields generated at any point across the cavity are to be added to $E_0$ to which we assign the reference phase of 0°. We have assumed that the round trip phase shift, *2ϑ=2kd*, is almost an integral multiple of 2π radians, but there is a lagging phase angle labeled by *φ* and related to $kd$ by

$$2\theta = 2kd = q2\pi - \varphi \tag{7}$$

where q is an integer and $\vartheta$ is the electrical (or optical) length of the cavity, that is equal to $\frac{\omega n d}{c}$.

For $\varphi = 0$, we get the resonance condition that is

$$k \cdot 2d = \frac{\omega n \cdot 2d}{c} = \frac{2\pi \cdot 2d}{\lambda} = q \cdot 2\pi \tag{8.a}$$

Or

$$L = q \cdot \lambda \tag{8.b}$$

where $L = 2\lambda$, the cavity length, and $\lambda = \lambda_0/n$. This means that there has to be an integer number of half the wavelength (λ/2) between the two mirrors. So q is a very large number for optical frequencies and usual size cavities.

*Equation (8.*a*)* can be interpreted in terms of frequency *v* as

$$k \cdot 2d = \omega \cdot \frac{2nd}{c} = 2\pi f \cdot \frac{2nd}{c} = q \cdot 2\pi \tag{9.a}$$

or

$$f = q\frac{c}{2nd} = q\frac{c/n}{L} \tag{9.b}$$

And as q is an integer number, this means that there are only discrete resonant frequencies. So, two consecutive resonant frequencies are at certain frequency difference that is called *Free Spectral Range (FSR)*

$$(FSR) = f_{q+1} - f_q = \frac{c}{2nd} = \frac{c/n}{L} \tag{9.c}$$

We can derive the transmission, $T(\theta)\ or\ T(f)$, of this two-mirror cavity we study in terms of the optical length ($\vartheta$) or of frequency ($f$), respectively, by defying the electric field inside it. Therefore, after some mathematical operations, we obtain

$$T(\theta) = \frac{(1-R_1)(1-R_2)}{\left(1-\sqrt{R_1R_2}\right)^2 + 4\sqrt{R_1R_2}\sin^2\theta} \tag{10.a}$$

where $R_1$ and $R_2$ is the power reflectivity coefficient of the input and output mirrors, respectively. By changing the variable $\vartheta$ to $\frac{2\pi(f-f_q)}{c}\frac{L}{2}$, where $f_q$ is the frequency of the cavity resonances, and by taking into consideration some definitions below of the *survival factor* ($A$) and the *finesse* ($\mathcal{F}$) we get the following expression of the cavity's transmission in terms of frequency

$$T(f) = \frac{(1-R_1)(1-R_2)}{(1-A)^2} \cdot \frac{1}{1+\left(\frac{2F}{\pi}\right)^2 \sin^2\frac{2\pi(f-f_q)}{c}\frac{L}{2}} \tag{10.b}$$

The survival factor per round-trip for the two-mirror cavity is $A = \sqrt{R_1R_2(1-cavity\ losses)}$ and $F$ is the *Finesse*, a quantity that measures the filtering properties of the cavity, and is defined as

$$F = \frac{FSR}{FWHM} = \frac{\pi\sqrt{A}}{1-A} \tag{11}$$

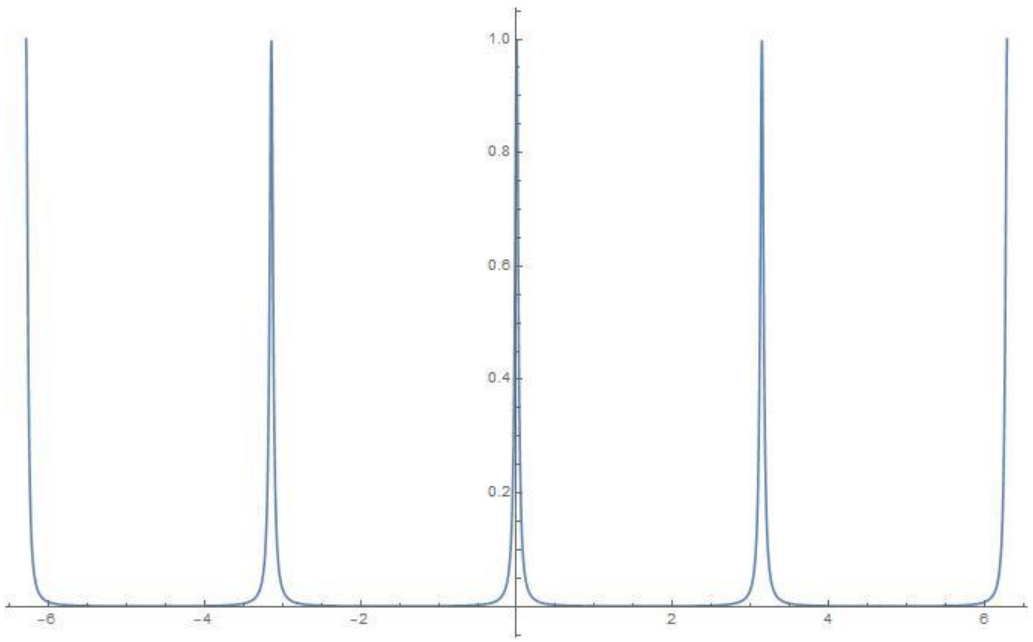


*Figure 5: Transmission spectrum of the cavity for $R_1 = R_2 = 0.95$ with optical length from -2π to 2π*

The transmission spectrum of a two-mirror cavity with reflectivity of the mirrors $R_1 = R_2 = 0.95$ is shown in *Figure 5* as a function of the optical length in the range $\theta = [-2\pi, 2\pi]$. Also, the transmission spectrum of the two-mirror cavity is depicted in *Figure 6* for different reflectivity of the cavity's mirrors (here we also assume $R_1 = R_2$).

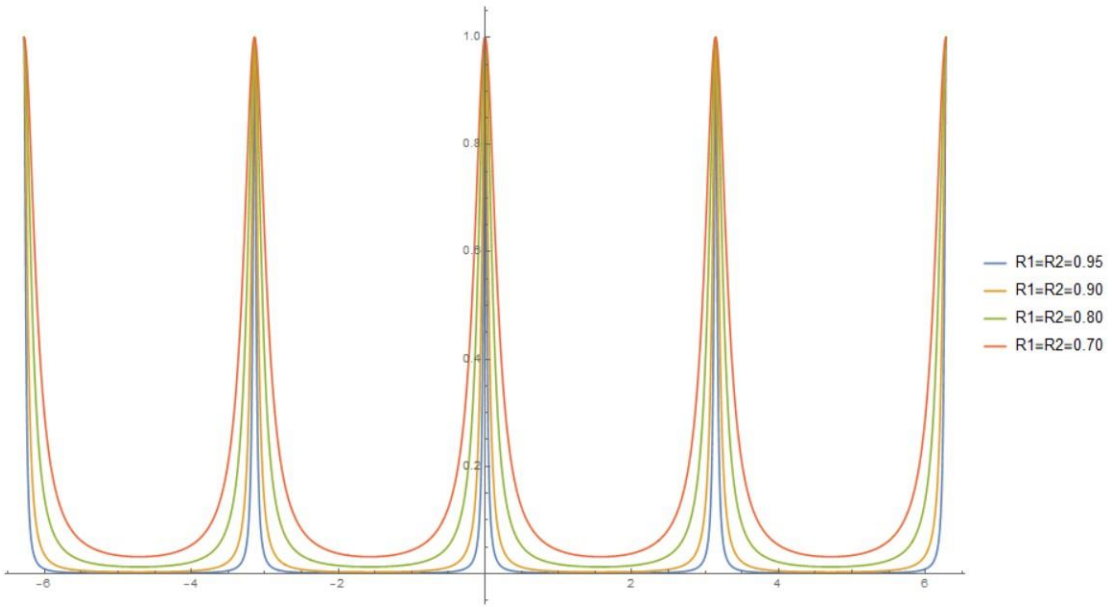


*Figure 6: Transmission spectrum of the cavity for different reflectivity of the cavity's mirrors with optical length from -2π to 2π*

To derive a formula for the *full width at half maximum (FWHM)* of the resonance we find the two frequencies ($f_+$ and $f_-$ for greater and smaller frequency than the resonance, respectively) at which the transmission function gets half the maximum value corresponding to the resonance and therefore the *FWHM* is estimated to

$$\Delta f_{1/2} = \frac{FSR}{\pi}\frac{1-A}{\sqrt{A}} \tag{12}$$

## Atomic Transitions

Light inside the cavity interacts with the intracavity samples, in our case atomic iodine. We present the general theory of interaction between light and matter. In this section we will discuss the relevant EM theory, which leads to absorption and stimulated emission of radiation, via electric dipole or other, *forbidden*, interactions.

### Electromagnetic force and Maxwell's equations

Electromagnetic force (or interaction) is one of the four fundamental interactions in nature. Its interaction between atomic nuclei and their orbital electrons holds atoms together and is also responsible for the chemical bonds between atoms which create molecules, and intermolecular forces. It governs all chemical processes, which arise from interactions between the electrons of neighboring atoms.

The theory of how electric and magnetic fields are generated by each other and by charges and currents is mathematically described by Maxwell's equations. The equations introduce the electric field, $E$ (vector field), and the magnetic field (or magnetic-flux density), $B$ (pseudovector field), each generally having a time and location dependence. Maxwell's equations in matter (also called macroscopic) are in the table below:

**Table 1:** Maxwell's equations in matter

| Name | Differential equations |
|---|---|
| Gauss's law | $\nabla \cdot \boldsymbol{D} = \rho_f$ |
| Gauss's law for magnetism | $\nabla \cdot \boldsymbol{B} = 0$ |
| Maxwell-Faraday equation (Faraday's law of induction) | $\nabla \times \boldsymbol{E} = -\frac{\partial \boldsymbol{B}}{\partial t}$ |
| Ampère's circuital law (with Maxwell's addition) | $\nabla \times \boldsymbol{H} = \boldsymbol{J_f} + \frac{\partial \boldsymbol{D}}{\partial t}$ |

The universal constants (S.I. units) appearing in the equations are the permittivity of free space, $\varepsilon_0$, the permeability of free space, $\mu_0$, and the speed of light, $c = 1/\sqrt{\varepsilon_0 \mu_o}$. Also, $\boldsymbol{D} \equiv \varepsilon_0 \boldsymbol{E} + \boldsymbol{P}$ is the electric displacement, where $\boldsymbol{P}$ is the polarization field and $\boldsymbol{H} = \frac{1}{\mu_0}\boldsymbol{B}$+**M** the magnetic field strength (or magnetizing field), where $\boldsymbol{M}$ is the magnetization field, while $\boldsymbol{J_f}$ and $\rho_f$ are the densities of currents and free charges, respectively.

For a linear isotropic dielectric material, the polarization is given by $\boldsymbol{P} = \varepsilon_0 \chi_e \boldsymbol{E} = \varepsilon_0(\varepsilon_r - 1)\boldsymbol{E}$, where $\chi_e$ is the electric susceptibility that indicates the degree of polarization of a dielectric material in response to an applied electric field. The electric permittivity of the material is $\varepsilon = \varepsilon_r \varepsilon_0 = (1 + \chi_e)\varepsilon_0$, and its permeability is $\mu = \mu_0 \mu_r = \mu_0(1 + \chi_m)$, where $\varepsilon_r$ and $\mu_r$ are the relative permittivity and relative permeability, respectively, and $\chi_m$ is the magnetic susceptibility of the medium. The permittivity $\varepsilon$ and permeability $\mu$ of a medium together determine the phase velocity $v = c/n$ of electromagnetic radiation through that medium that is $\varepsilon\mu = 1/v^2$. So, the product $\varepsilon\mu$ defines the refraction index of the medium as $n = \sqrt{(1 + \chi_e)(1 + \chi_m)}$ for a linear isotropic dielectric medium. Therefore, the polarizability of a medium affects the velocity of light as it passes through it, that is related to the refractive index of the medium.

Electric and magnetic field can be expressed in terms of a scalar potential, $\varphi$, and a vector potential, $A$, as

$$\boldsymbol{B} = \boldsymbol{\nabla} \times \boldsymbol{A}$$
$$\boldsymbol{E} = -\nabla\varphi - \frac{\partial \boldsymbol{A}}{\partial t} \tag{13}$$

I f we choose to work with the Coulomb gauge, that is $\nabla \cdot \boldsymbol{A} = 0$, and with $\varphi = 0$, then the previous equations become:

$$\boldsymbol{B} = \boldsymbol{\nabla} \times \boldsymbol{A}$$
$$\boldsymbol{E} = -\frac{\partial \boldsymbol{A}}{\partial t} \tag{14}$$

By substituting Equation (14) into the Ampere's law we get the wave equation for the vector field, $A$, that is

$$\left(\nabla^2 - \frac{1}{c^2}\frac{\partial^2}{\partial t^2}\right)\boldsymbol{A} = 0 \tag{15}$$

where $c = 1/\sqrt{\varepsilon_0\mu_0}$ is the speed of light in vacuum.

From the above equations we can express the quantities $\boldsymbol{A}(\boldsymbol{r},t)$, $\boldsymbol{E}(\boldsymbol{r},t)$, and $\boldsymbol{B}(\boldsymbol{r},t)$ for a simple wave as

$$\boldsymbol{A}(\boldsymbol{r},t) = \boldsymbol{\varepsilon}\frac{E_0}{\sqrt{2}i\omega}e^{i(\boldsymbol{k}\cdot\boldsymbol{r}-\omega t)}$$
$$\boldsymbol{E}(\boldsymbol{r},t) = \boldsymbol{\varepsilon}\frac{E_0}{\sqrt{2}}e^{i(\boldsymbol{k}\cdot\boldsymbol{r}-\omega t)} \tag{16}$$
$$\boldsymbol{B}(\boldsymbol{r},t) = -\boldsymbol{b}\frac{E_0}{\sqrt{2}c}e^{i(\boldsymbol{k}\cdot\boldsymbol{r}-\omega t)}$$

where $E_0$ is a constant, $c$ is the speed of light in vacuum, $\boldsymbol{\varepsilon}$ is the electric polarization vector, and $\boldsymbol{b}$ is the wave's magnetic component direction. From electromagnetic theory we know that the following relations are satisfied; $\boldsymbol{\varepsilon}\cdot\boldsymbol{b} = 0$ and $\mathbf{b} = \mathbf{n}\times\boldsymbol{\varepsilon}$, where $\boldsymbol{n}$ is the wave's direction of propagation. The symbol $k$ is the wavenumber vector pointing in the propagation direction and is defined as $\boldsymbol{k} = k\boldsymbol{n} = \frac{\omega}{c}\boldsymbol{n} = \frac{2\pi}{\lambda}\boldsymbol{n}$ ($\lambda$ is the wave's wavelength, and $\omega = 2\pi/\lambda$ is the angular frequency of the described wave).

## Transitions rates (from time-dependent perturbation theory) [5]

A harmonic perturbation of the type

$$H_1(t) = Vexp(i\omega t) + V^{\dagger}\exp(-i\omega t) \tag{17}$$

gives rise to two different processes; the stimulated emission of a photon of energy $\hbar\omega$ while making a transition to a lower energy state of the system (due to the $\exp(-i\omega t)\ term$), and the absorption of a photon of energy $\hbar\omega$ while making a transition to a higher energy state (due to the $\exp(i\omega t)\ term$).

The transition probability per unit time (transition rate) from a state $|i>$ to a state $|f>$ is given by the Fermi's golden rule (with time-dependent perturbation theory). Therefore, the transition rates for the stimulated emission and for the absorption are

$$w^{stm}_{i\to|f|} = \frac{2\pi}{\hbar}\overline{|V_{fi}|^2}\rho(E_f)|_{E_f=E_i-\hbar\omega} \ \ or \ \ \frac{2\pi}{\hbar}\overline{|V_{fi}|^2}\delta(E_f - E_i + \hbar\omega) \tag{18}$$
$$w^{abs}_{i\to|f|} = \frac{2\pi}{\hbar}\overline{\left|V^{\dagger}_{fi}\right|^2}\rho(E_f)|_{E_f=E_i+\hbar\omega} \ \ or \ \ \frac{2\pi}{\hbar}\overline{\left|V^{\dagger}_{fi}\right|^2}\delta(E_f - E_i - \hbar\omega) \tag{19}$$

respectively, where $\overline{|V_{fi}|^2}$ is the average of $|V_{fi}|^2$ over all final states with approximately the same energy as the initial state, $V_{fi} =< f|V|i >$, and $\rho(E)$ is the density of states with energy E. The formula that contains the delta function must be integrated with $\int dE_f\ (\dots)\rho(E_f)$. From the equations above we can extract the equation below:

$$\frac{w_{i\to|f|}^{stm}}{\rho(E_f)} = \frac{w_{|f|\to i}^{abs}}{\rho(E_i)} \tag{20}$$

that expresses a fundamental symmetry between absorption and simulated emission that is called detailed balance.

## Absorption and Stimulated Emission of Radiation [5]

The interaction between an electron of a hydrogen-like atom and the classical electromagnetic (EM) radiation can described using time-dependent perturbation theory (TDPT). The Hamiltonian of such interaction is

$$\begin{aligned} H &= \frac{(\boldsymbol{p}+e\boldsymbol{A})^2}{2m} - e\varphi(\boldsymbol{r}) + V \\ &= \frac{\boldsymbol{p}^2}{2m} + \frac{e\boldsymbol{A}\cdot\boldsymbol{p}}{m} + \frac{e^2A^2}{2m} - e\varphi(\boldsymbol{r}) + V \end{aligned} \tag{21}$$

where $m$, $e$ and $\boldsymbol{p}$ are the mass, charge and momentum of the atomic electron, $V$ is the atomic potential energy, while $\varphi$ and $\boldsymbol{A}$ are the scalar and vector potential of the EM field. In the Coulomb gauge, where $[\boldsymbol{p},\boldsymbol{A}] = 0$, the Hamiltonian in the previous equation (with $\boldsymbol{A}^2$ term omitted) becomes

$$H = \frac{\boldsymbol{p}^2}{2m} + \frac{e\boldsymbol{A}\cdot\boldsymbol{p}}{m} + V \tag{22}$$

Suppose that we work with a monochromatic plane wave of angular frequency $\omega$, for which

$$\boldsymbol{A} = 2A_0\boldsymbol{\varepsilon}\cos\left(\frac{\omega}{c}\boldsymbol{n}\cdot\boldsymbol{r} - \omega t\right) = A_0\boldsymbol{\varepsilon}\left(e^{i\frac{\omega}{c}\boldsymbol{n}\cdot\boldsymbol{r}-i\omega t} + e^{-i\frac{\omega}{c}\boldsymbol{n}\cdot\boldsymbol{r}+i\omega t}\right) \tag{23}$$

where $2A_0$ is the amplitude of the vector potential.

We can separate the Hamiltonian we mentioned above in an unperturbed part, $H_0$, and a small perturbation, $H_1 \ll H_0$. It is $H = H_0 + H_1$, where

$$H_0 = \frac{\boldsymbol{p}^2}{2m} + V \tag{24}$$

$$H_1 \approx \frac{e\boldsymbol{A}\cdot\boldsymbol{p}}{m} = \frac{eA_0}{m}\left(e^{i\frac{\omega}{c}\boldsymbol{n}\cdot\boldsymbol{r}-i\omega t} + e^{-i\frac{\omega}{c}\boldsymbol{n}\cdot\boldsymbol{r}+i\omega t}\right)\boldsymbol{\varepsilon}\cdot\boldsymbol{p} \tag{25}$$

We define the quantity below which has length dimensions

$$\boldsymbol{d}_{if} = \frac{-i}{m\omega_{if}}\langle i\left|\exp\left[i\frac{\omega}{c}\boldsymbol{n}\cdot\boldsymbol{r}\right]\boldsymbol{p}\right|f\rangle \tag{26}$$

where $\omega_{if} = \frac{E_i - E_f}{\hbar}$, with $E_i$ the energy of the initial state and $E_f$ the energy of the final state.

From analogous with the TDPT for harmonic perturbation, it follows that the absorption and stimulated emission rates on a specific angular frequency, $\omega$, are

$$w_{i\to f}^{abs} = 2\pi\frac{e^2\omega_{fi}^2}{\hbar^2}|A_0|^2\left|\boldsymbol{\varepsilon}\cdot\boldsymbol{d}_{fi}\right|^2\delta(\omega-\omega_{fi}) \tag{27}$$

$$w_{i\to f}^{stm} = 2\pi \frac{e^2\omega_{if}^2}{\hbar^2}|A_0|^2\left|\boldsymbol{\varepsilon}\cdot\boldsymbol{d}_{if}\right|^2\delta(\omega-\omega_{if}) \tag{28}$$

respectively. We mention that the peak electric, magnetic and vector field strengths are connected via the relations

$$B_0 = \frac{E_0}{c} = \frac{2A_0\omega}{c} \tag{29}$$

Thus, the absorption and stimulated emission cross-section are

$$\sigma_{i\to f}^{abs}(\omega) = 4\pi^2\alpha\omega\left|\boldsymbol{\varepsilon}\cdot\boldsymbol{d}_{fi}\right|^2\delta(\omega-\omega_{fi}) \tag{30}$$

$$\sigma_{i\to f}^{stm}(\omega) = 4\pi^2\alpha\omega\left|\boldsymbol{\varepsilon}\cdot\boldsymbol{d}_{if}\right|^2\delta(\omega-\omega_{if}) \tag{31}$$

respectively.

## Electric Dipole Transitions (E1)

The electric dipole transitions are based on the assumption that the wavelength of the EM radiation that interacts with the atom in the context of atomic transitions is much larger than the size of a light atom. So, it is possible to expand the exponential term that appears in the relation:

$$\boldsymbol{d}_{if} = \frac{-i}{m\omega_{if}}\langle i\left|\exp\left[i\frac{\omega}{c}\boldsymbol{n}\cdot\boldsymbol{r}\right]\boldsymbol{p}\right|f\rangle \tag{32}$$

to the series

$$exp\left(i\frac{\omega}{c}\boldsymbol{n}\cdot\boldsymbol{r}\right) = 1 + i\frac{\omega}{c}\boldsymbol{n}\cdot\boldsymbol{r} + \cdots \tag{33}$$

and to be approximated by the leading term, that is unity, in the electric dipole approximation.

In this approximation it is

$$\boldsymbol{d}_{if} \approx \frac{-i}{m\omega_{if}}\langle i|\boldsymbol{p}|f\rangle \tag{34}$$

Keeping in mind basic equations from quantum mechanics such as $[\boldsymbol{r}, H_0] = \frac{i\hbar\boldsymbol{p}}{m}$, then

$$\langle i|\boldsymbol{p}|f\rangle = -i\frac{m}{\hbar}\langle i|[\boldsymbol{r}, H_0]|f\rangle = im\omega_{if}\langle i|\boldsymbol{r}|f\rangle \tag{35}$$

which implies that

$$\boldsymbol{d}_{if} \approx \langle i|\boldsymbol{r}|f\rangle \tag{36}$$

This is the electric dipole matrix element. The electric dipole operator is defined as

$$\boldsymbol{D} = e\,\boldsymbol{r} \tag{37}$$

In order for a transition to be allowed, this matrix element must be non-zero. This gives rise to the E1 selection rules below, which guarantee that the aforementioned condition holds true.

$$\Delta l = \pm 1, \qquad \Delta m = 0, \pm 1, \qquad \Delta m_s = 0 \tag{38}$$

where $l$ is the azimuthal quantum number, $m$ is the magnetic quantum number, $m_s$ is the spin quantum number, or

$$\Delta j = 0, \pm 1, \qquad \Delta m_j = 0, \pm 1 \tag{39}$$

where $j$ is the standard quantum number defined as $j = l + s$, and $m_j$ is $j$'s projection along the z-axis. We expect the $\boldsymbol{d}_{if}$ to be of order $a_0$ (Bohr radius) for low lying hydrogen transitions. We define the dimensionless oscillator strength term that is

$$F_{if} = \frac{2m\omega_{fi}}{\hbar} |\langle i|\boldsymbol{r}|f\rangle|^2 \tag{40}$$

and when it is summed over all atomic states (provided that the initial state is the ground state) it gives us unity, and that is the Thomas-Reiche-Kuhn sum rule

$$\sum_f F_{if} = 1 \tag{41}$$

So, the net absorption cross-section is calculated

$$\int_{-\infty}^{+\infty} d\omega \sum_f \sigma_{i\to f}^{abs}(\omega) = 2\pi^2 \alpha \frac{\hbar}{m} \sum_f F_{if} \tag{42}$$

and, provided that $i$ is the ground state, the above expression is simplified to

$$\int_{-\infty}^{+\infty} d\omega \sum_f \sigma_{i\to f}^{abs}(\omega) = 2\pi^2 \alpha \frac{\hbar}{m} = 2\pi^2 r_e c \tag{43}$$

where $r_e = e^2/(4\pi\varepsilon_0 mc^2)$ is the classical electron radius.

## Forbidden Transitions

If we keep the two first terms when expanding the exponential regarding that the wavelength of the EM radiation emitted or absorbed by the atom is much larger than the dimensions of the atom, then the product $\boldsymbol{\varepsilon} \cdot \boldsymbol{d}_{if}$ (assumed that $\omega = \omega_{if}$) becomes

$$\boldsymbol{\varepsilon} \cdot \boldsymbol{d}_{if} = \boldsymbol{\varepsilon} \frac{-i}{m\omega_{if}} \left\langle i \left| \exp\left[i \frac{\omega}{c} \boldsymbol{n} \cdot \boldsymbol{r}\right] \boldsymbol{p} \right| f \right\rangle \approx \langle i|\boldsymbol{\varepsilon} \cdot \boldsymbol{r}|f\rangle + \frac{1}{mc} \langle i|(\boldsymbol{n} \cdot \boldsymbol{r})(\boldsymbol{\varepsilon} \cdot \boldsymbol{p})|f\rangle \tag{44}$$

The second term on the right hand of the above equation is of order $\alpha a_0 \ll a_0$, that is far less than the $a_0$ order of the first term and stands for an electric dipole transition. So, if we suppose that we study a transition that is electric-dipole-forbidden due to the selection rules, then this first term vanishes and only the second term of the product $\boldsymbol{\varepsilon} \cdot \boldsymbol{d}_{if}$ survives, that we will see stands for magnetic dipole and electric quadrupole transitions.

The orbital momentum is given by the relation $\boldsymbol{L} = \boldsymbol{r} \times \boldsymbol{p}$, so that $\boldsymbol{b} \times \boldsymbol{L} = (\boldsymbol{n} \cdot \boldsymbol{r})(\boldsymbol{\varepsilon} \cdot \boldsymbol{p}) - (\boldsymbol{\varepsilon} \cdot \boldsymbol{r})(\boldsymbol{n} \cdot \boldsymbol{p})$.

If we define an operator $\boldsymbol{S}$ as

$$\boldsymbol{S} = \frac{im}{\hbar} [H, (\boldsymbol{\varepsilon} \cdot \boldsymbol{r})(\boldsymbol{n} \cdot \boldsymbol{r})] \tag{45a}$$

this can be expressed as

$$\boldsymbol{S} = (\boldsymbol{\varepsilon} \cdot \boldsymbol{r})(\boldsymbol{n} \cdot \boldsymbol{p}) + (\boldsymbol{n} \cdot \boldsymbol{r})(\boldsymbol{\varepsilon} \cdot \boldsymbol{p}) \tag{45b}$$

so that we can extract the relation

$$(\boldsymbol{n} \cdot \boldsymbol{r})(\boldsymbol{\varepsilon} \cdot \boldsymbol{p}) = \frac{1}{2} \boldsymbol{b} \cdot \boldsymbol{L} + \frac{im}{2\hbar} [H, (\boldsymbol{\varepsilon} \cdot \boldsymbol{r})(\boldsymbol{n} \cdot \boldsymbol{r})] \tag{46}$$

Hence the dot product $\boldsymbol{\varepsilon} \cdot \boldsymbol{d}_{if}$ on *Equation (42)*, supposed that we have an electric dipole forbidden transition, becomes

$$\boldsymbol{\varepsilon}\cdot\boldsymbol{d_{if}}=\frac{1}{2mc}\boldsymbol{b}\cdot\langle i|\boldsymbol{L}|f\rangle+\frac{i\omega_{if}}{2c}\boldsymbol{\varepsilon}\cdot\boldsymbol{Q}_{if}\cdot\boldsymbol{n} \tag{47a}$$

where $\boldsymbol{Q}_{if}$ is a traceless tensor defined as

$$\left(\boldsymbol{Q_{if}}\right)_{jk}=\langle i|x_jx_k-\frac{r^2\delta_{jk}}{3}|f\rangle \tag{47b}$$

and $r^2=x_jx_j$. The two terms on the right hand of *Equation (47a)* give rise to completely different selection rules. Specifically, the first term is related with *magnetic dipole transitions* while the second with *electric quadrupole transitions*.

### *Magnetic Dipole Transitions (M1)*

The term in *Equation (47a)* (first term on the right side) associated with magnetic dipole transitions is incomplete because it lacks the interaction of the magnetic component of the EM wave with the electron's magnetic moment, described by the term

$$\delta H=-\boldsymbol{\mu}\cdot\boldsymbol{B}=\frac{e}{m}\boldsymbol{S} \tag{48}$$

where $\boldsymbol{S}$ is the electron spin. So, the additional contribution of the above interaction to $\boldsymbol{\varepsilon}\cdot\boldsymbol{d_{if}}$ (assumed again that $\omega=\omega_{if}$) is

$$\frac{1}{mc}\boldsymbol{b}\cdot\langle i|\boldsymbol{S}|f\rangle \tag{49}$$

and the magnetic dipole transitions can be completely described by the quantity

$$\boldsymbol{\varepsilon}\cdot\boldsymbol{d_{if}}=\frac{1}{2mc}\boldsymbol{b}\cdot\boldsymbol{M_{if}} \tag{50}$$

where $\boldsymbol{M_{if}}=\langle i|\boldsymbol{M}|f\rangle=\langle i|\boldsymbol{L}+2\boldsymbol{S}|f\rangle$, is the magnetic dipole matrix element, and $\boldsymbol{b_{1,2}}=\boldsymbol{n}\times\boldsymbol{\varepsilon_{1,2}}$, where $\boldsymbol{\varepsilon_{1,2}}$ are the two independent electric polarization vectors of the photon and it is $b_1=\varepsilon_2$ and $b_2=-\varepsilon_1$.

The magnetic dipole operator is

$$\boldsymbol{M}=\boldsymbol{L}+2\boldsymbol{S} \tag{51}$$

The selection rules that rise for magnetic dipole transitions are

$$\Delta l=0,\qquad \Delta m=0,\pm1,\qquad \Delta m_s=0,\pm1 \tag{52}$$

or

$$\Delta j=0,\pm1,\qquad \Delta m_j=0,\pm1 \tag{53}$$

while transitions between two $j=0$ states are forbidden.

### *Electric Quadrupole Transitions (E2)*

The term associated with electric quadrupole transitions is the second on the right hand in *Equation (47a)* that is repeated below

$$\boldsymbol{\varepsilon}\cdot\boldsymbol{d_{if}}=\frac{i\omega_{if}}{2c}\boldsymbol{\varepsilon}\cdot\boldsymbol{Q}_{if}\cdot\boldsymbol{n} \tag{54a}$$

where $\boldsymbol{Q}_{if}$ is the electric quadrupole matrix element defined previously as

$$\left(\boldsymbol{Q_{if}}\right)_{jk}=\langle i|\boldsymbol{r_j}\boldsymbol{r_k}-\frac{r^2\delta_{jk}}{3}|f\rangle \tag{54b}$$

and $r^2=x_jx_j$. The selection rules that govern this type of transition are

$$\Delta l = 0, \pm 2, \qquad \Delta m = 0, \pm 1, \pm 2, \qquad \Delta m_s = 0 \tag{55}$$

or

$$\Delta j = 0, \pm 1, \pm 2, \qquad \Delta m_j = 0, \pm 1, \pm 2 \tag{56}$$

while transitions between two $j = 0$ states, two $j = 1/2$, or a $j = 1$ and a $j = 0$ state, are forbidden.

For an electric quadrupole transition in a hydrogen atom, it is expected for $\boldsymbol{Q_{if}}$ to be of order $a_0^2$ ($a_0$ is the Bohr radius).

## Selection Rules

As we choose higher orders of the exponential we are lead to higher order transitions that give rise to different selection rules. The selection rules for some significant transitions are concentrated in *Figure 6*, derived from Wikipedia.

| Allowed transitions | | Electric dipole (E1) | Magnetic dipole (M1) | Electric quadrupole (E2) | Magnetic quadrupole (M2) | Electric octupole (E3) | Magnetic octupole (M3) |
|---|---|---|---|---|---|---|---|
| Rigorous rules | (1) | $\Delta J = 0, \pm 1$ $(J = 0 \nleftrightarrow 0)$ | | $\Delta J = 0, \pm 1, \pm 2$ $(J = 0 \nleftrightarrow 0, 1;\ \frac{1}{2} \nleftrightarrow \frac{1}{2})$ | | $\Delta J = 0, \pm 1, \pm 2, \pm 3$ $(0 \nleftrightarrow 0, 1, 2;\ \frac{1}{2} \nleftrightarrow \frac{1}{2}, \frac{3}{2};\ 1 \nleftrightarrow 1)$ | |
| | (2) | $\Delta M_J = 0, \pm 1$ $(M_J = 0 \nleftrightarrow 0$ if $\Delta J = 0)$ | | $\Delta M_J = 0, \pm 1, \pm 2$ | | $\Delta M_J = 0, \pm 1, \pm 2, \pm 3$ | |
| | (3) | $\pi_\mathrm{f} = -\pi_\mathrm{i}$ | $\pi_\mathrm{f} = \pi_\mathrm{i}$ | | $\pi_\mathrm{f} = -\pi_\mathrm{i}$ | | $\pi_\mathrm{f} = \pi_\mathrm{i}$ |
| LS coupling | (4) | One electron jump $\Delta L = \pm 1$ | No electron jump $\Delta L = 0,$ $\Delta n = 0$ | None or one electron jump $\Delta L = 0, \pm 2$ | One electron jump $\Delta L = \pm 1$ | One electron jump $\Delta L = \pm 1, \pm 3$ | One electron jump $\Delta L = 0, \pm 2$ |
| | (5) | If $\Delta S = 0$ $\Delta L = 0, \pm 1$ $(L = 0 \nleftrightarrow 0)$ | If $\Delta S = 0$ $\Delta L = 0$ | If $\Delta S = 0$ $\Delta L = 0, \pm 1, \pm 2$ $(L = 0 \nleftrightarrow 0, 1)$ | | If $\Delta S = 0$ $\Delta L = 0, \pm 1, \pm 2, \pm 3$ $(L = 0 \nleftrightarrow 0, 1, 2;\ 1 \nleftrightarrow 1)$ | |
| Intermediate coupling | (6) | If $\Delta S = \pm 1$ $\Delta L = 0, \pm 1, \pm 2$ | | If $\Delta S = \pm 1$ $\Delta L = 0, \pm 1,$ $\pm 2, \pm 3$ $(L = 0 \nleftrightarrow 0)$ | If $\Delta S = \pm 1$ $\Delta L = 0, \pm 1$ $(L = 0 \nleftrightarrow 0)$ | If $\Delta S = \pm 1$ $\Delta L = 0, \pm 1,$ $\pm 2, \pm 3, \pm 4$ $(L = 0 \nleftrightarrow 0, 1)$ | If $\Delta S = \pm 1$ $\Delta L = 0, \pm 1,$ $\pm 2$ $(L = 0 \nleftrightarrow 0)$ |

*Figure 7: Selection Rules. Table- derived form Wikipedia*

where $\pi = (-1)^l$ is the parity of each state and the symbol $\nleftrightarrow$ is used to indicate a forbidden transition.

## Iodine

Atomic Iodine ($Z = 53$) is the fourth member of halogen group with 53 electrons and one stable isotope, $^{127}$I. Its electronic configuration is [Kr]4d$^{10}$5s$^2$5p$^5$. It has non-zero nuclear spin, $I = 5/2$, that produces hyperfine splitting.

As summarized in [6], in the LS coupling approximation the p shell has an orbital angular momentum quantum number $L = 1$ and spin quantum number $S = 1/2$. The combination of these two (either parallel or antiparallel) forms a fine structure doublet that consists of the states $^2P_{1/2}$ and $^2P_{3/2}$.

Different possible orientations of the nuclear angular momentum ($I$) with respect to the orbital angular momentum ($J$) result in total angular momentum quantum numbers, $F$, where

$$\boldsymbol{F} = \boldsymbol{I} + \boldsymbol{J} \tag{57}$$

The fine structure levels with specific quantum number $\boldsymbol{J}$ and energy $\boldsymbol{E_J}$, will split into sublevels with different quantum number $\boldsymbol{F}$ and energy $\boldsymbol{E_F}$, that form the hyperfine structures.

The upper level ($^2P_{1/2}$) with $J = 1/2$ splits in two hyperfine sublevels with $F = 2, 3$, while the lower level ($^2P_{3/2}$) with $J = 3/2$ splits in four hyperfine sublevels with $F = 1, 2, 3, 4$.

The energy of the multiplet of the hyperfine structure is given by

$$\frac{E_F}{\hbar} = \frac{E_J}{\hbar} + \frac{K}{2}A + \frac{3K(K+1) - 4IJ(I+1)(J+1)}{8IJ(2I-1)(2J-1)}B \tag{58}$$

$$K = F(F+1) - I(I+1) - J(J+1) \tag{59}$$

where $A$ is the magnetic dipole coupling constant, and $B$ is the electric quadrupole hyperfine interaction constant.

For atomic iodine these constants are determined in the Table below [4]:

**Table 2:** Hyperfine coupling constants for ground and excited state of atomic iodine

| Total angular momentum $J$ | Hyperfine coupling constants | |
|---|---|---|
| | Magnetic dipole [GHz] | Electric quadrupole [GHz] |
| Ground state $J = 3/2$ | 0.83274 | 1.080366 |
| Excited state $J = 1/2$ | 6.669503 | 0 |

There are 6 magnetic dipole transitions between the hyperfine sublevels that are divided into two groups of 3 lines, where each group ends up to a different upper level. Therefore, if we use symbols $F$ and $F'$ to indicate the total angular momentum quantum number of the initial and final state of a transitions, respectively, then we have the following $F \to F'$ transitions: $1,2,3 \to 2$ and $2,3,4 \to 3$.

The energy level structure of the $5\ ^2P_{3/2} \to 5\ ^2P_{1/2}$ M1 transitions of atomic $^{127}$I along with the calculated transmission spectrum of an IR laser as its frequency is scanned across the resonance has been calculated for specific parameters in [3], and are depicted in *Figure 11* (from [3]).

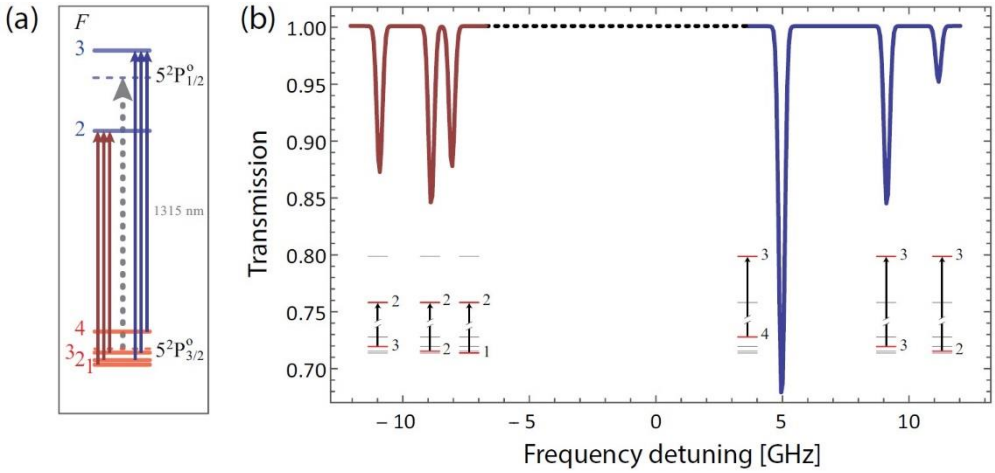


*Figure 8: (a) Energy level structure of the $5^2P_{3/2} \rightarrow 5^2P_{1/2}$ M1 transition of atomic $^{127}I$.*
*(b) Calculated transmission spectrum of an IR laser as its frequency is scanned across the resonance.*
*Figure from [3]*

The frequency of the nominal transition between the two fine structure levels is at 1315nm and is marked with the dashed lines in *Figure 11 (a)*.

## Beer-Lambert Law and Cross-Section

The generic light-matter interaction theory presented in the previous pages can now be made specific for the interaction of interest for this thesis, i.e., **the atomic, magnetic-dipole iodine transition $^2P_{3/2} \rightarrow {}^2P_{1/2}$ at 1315.34 nm** (in vacuum). We start by discussing the Beer-Lambert law, which governs light attenuation for light traversing an absorber.

Consider a photon beam of intensity $I_0$ and angular frequency $\omega$ passes through a medium with $N$ atoms per unit volume (number density). In a slice of the medium of thickness $\Delta z$ there are $N\Delta z$ atoms per unit area. Then, $N\sigma\Delta z$ is the intensity fraction of the initial photon beam that is absorbed by the atoms, where $\sigma$ is the cross-section area that represents the 'target' area of each atom. The term $N\sigma\Delta z$ also represents the fraction of the target area that is covered by atoms, which corresponds to the probability of a photon of the beam to hit a target atom [Foot, Section 7.6, p.138]. The attenuation of the beam is described in the equation

$$\frac{dI}{I} = -adz = -N\sigma\Delta z \tag{60}$$

where $\alpha(\omega)$ is the absorption coefficient. By integration we get

$$I(z) = I_0 e^{-az} = I_0 e^{-N\sigma z} \tag{61}$$

This is the most commonly quoted form of the **Beer- Lambert Law**.

Therefore, when light passes through an absorptive medium of length $l$ we can define the transmission as the ratio of the intensity of transmitted ($I_{out}$) to incident ($I_{in}$) light.

$$T(\omega) = \frac{I_{out}}{I_{in}} = e^{-N\sigma(\omega)l} \tag{62}$$

The transmission is a function of frequency, where the frequency dependence is included in the cross section function, and reflects the level structure of the absorber. For an atomic system, as described in references [3,7], the cross section term for a specific $|F\rangle \rightarrow |F'\rangle$ hyperfine transition is given by:

$$\sigma(\omega) = \sigma_0 \sum_{F,F'} C_{FF'} \mathcal{V}''_{\mathrm{FF'}}(\omega) \tag{63}$$

where $\sigma_0$ is the *integrated absorption cross section*, $C_{FF'}$ contain the geometrical factors connecting $(J, I, F)$ *to* $(J', I, F')$, and $\mathcal{V}''_{\mathrm{FF'}}$ is the absorptive part of the Voigt profile:

$$\sigma_0 = \frac{\pi\mu_0\omega_{JJ'}}{\hbar c}\frac{1}{2J+1}\frac{M1^2}{3} \tag{64}$$

$$C_{FF'} = \frac{(2F+1)(2F'+1)}{2I+1}\begin{Bmatrix} J & 1 & J' \\ F' & I & F \end{Bmatrix}^2 \tag{65}$$

$$\mathcal{V}''_{\mathrm{FF'}}(\omega) = \frac{w'\left(\frac{\omega-\omega_{FF'}}{\Delta\omega_D}, \frac{\Gamma/2}{\Delta\omega_D}\right)}{\sqrt{\pi}\Delta\omega_D} \tag{66}$$

In the previous equations $\omega_{JJ'}$ is the nominal transition frequency, corresponding to 1315.34nm, $\omega_{FF'}$ is the frequency of a particular hyperfine $F \rightarrow F'$ transition, $J = \frac{3}{2}$, $J' = \frac{1}{2}$, $I = \frac{5}{2}$, $\{\dots\}$ denotes a 6J symbol, and $M1 \equiv \langle M1\rangle \equiv \langle J||\mu^{(1)}||J'\rangle = 1.15\ \mu_B$ [7] is the reduced matrix element of the magnetic dipole operator $\mu^{(1)}$. In the last equation $w'$ is the real part

of the Faddeeva function of a complex variable (the real and imaginary part of which are the arguments of $w'$ in Eq. (66)). Also, $\Gamma$ is the FWHM homogenous linewidth, and $\Delta\omega_D = \omega_{JJ'}\sqrt{2k_BT/(Mc^2)}$ is the Doppler half width at $1/e$ value where $k_B$ is the Boltzmann constant, $T$ the temperature, $M$ the mass of the atom, and $c$ the speed of light.

For this particular transition, selection rules, and the fact that $J = 3/2 > 1$, allow for an ***electric quadrupole*** contribution, which needs to be included in our treatment. As mentioned in [7], the electric quadrupole operator is

$$E2 = -\frac{q\omega}{4\sqrt{3}}\boldsymbol{Q}_{\boldsymbol{q}}^{\boldsymbol{E2}} \tag{67}$$

where $\boldsymbol{Q}_{\boldsymbol{q}}^{\boldsymbol{E2}}$ is the traceless tensor defined as $\boldsymbol{Q}_{if}$ in previous section, and $q = 0, \pm 1, \pm 2$ characterizes the projection component of the quadrupole tensor. We have to do the following replacement:

$$\frac{M1^2}{3} \to |\langle i|\boldsymbol{M} + \boldsymbol{E2}\,||f\rangle\,|^2 \tag{68}$$

Also, we define the electric quadrupole to magnetic dipole ratio parameter $\chi$ that is

$$\chi = \frac{\omega}{4\sqrt{3}}\frac{\left|\langle i\right||\boldsymbol{E2}|\left|f\rangle\right|}{\left|\langle i\right||\boldsymbol{M}|\left|f\rangle\right|} \tag{69}$$

and the difference with the cross section defined previously is the $C_{FF'} \to C'_{FF'}$ substitution of the geometrical factor with

$$C_{FF'} = \frac{(2F+1)(2F'+1)}{2I+1}\left(\begin{Bmatrix} J & 1 & J' \\ F' & I & F \end{Bmatrix}^2 + \frac{3\chi^2}{5}\begin{Bmatrix} J & 2 & J' \\ F' & I & F \end{Bmatrix}^2\right) \tag{70}$$

The electric quadrupole component of this particular transition, and, thus, the dimensionless parameter $\chi$, was first measured during the masters of E. Toutoudaki at our lab [4], and, again, during this thesis. Before these measurements, the value was only available through initial theoretical calculations performed by V. A. Dzuba (private communication). The coincidence of calculated and measured values is discussed later in the text.

In order to illustrate the transmission function for the M1 transitions in iodine, we plot the transmission function, coming from the Beer-lambert law, as a function of frequency with $\chi = 0$. We assume we have an absorptive medium of length $l = 123\ cm$ (which is the length of the iodine cell we used in the experiments), numeric density of atomic iodine $N = 0.89 \cdot 10^{15}\ \mathrm{cm}^{-3}$, Doppler half width at $1/e\ \Delta\omega_{\mathrm{D}} = 2\pi \cdot 148\ MHz$, FWHM homogenous linewidth $\Gamma = 2\pi \cdot 3\ MHz$, and we get the diagram below:

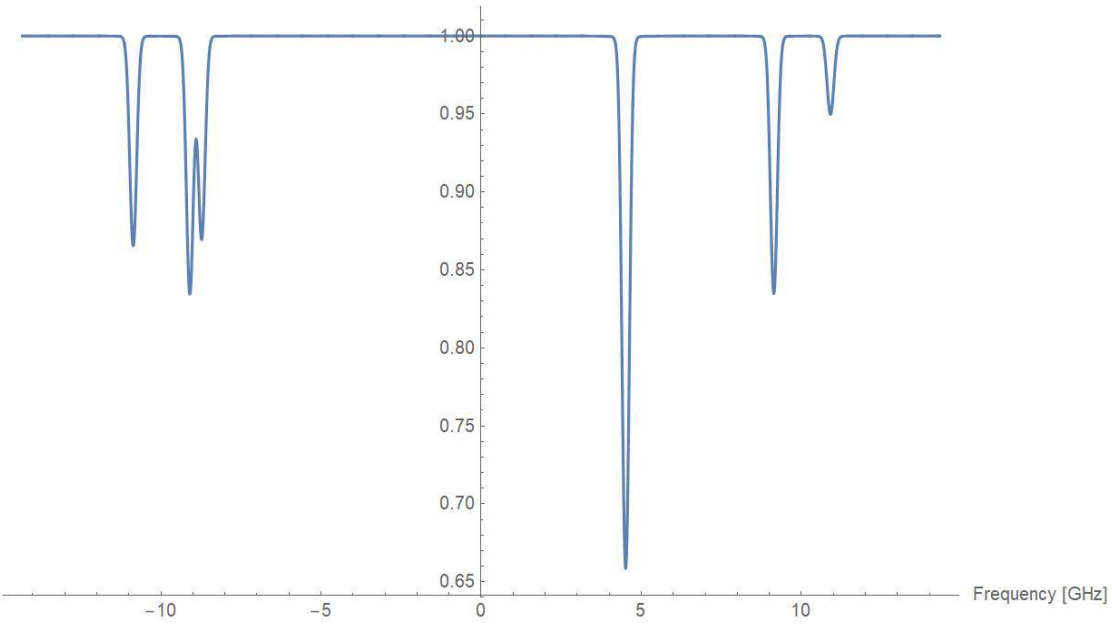


*Figure 9: Calculated transmission spectrum of the $5^2P_{3/2} \rightarrow 5^2P_{1/2}$ M1 transition of atomic $^{127}I$.*

To continue, if we want to include the E2 transitions we should assign a value to $\chi$. For the time being, and for illustration purposes, we set $\chi = 0.5$, which yields the following diagram:

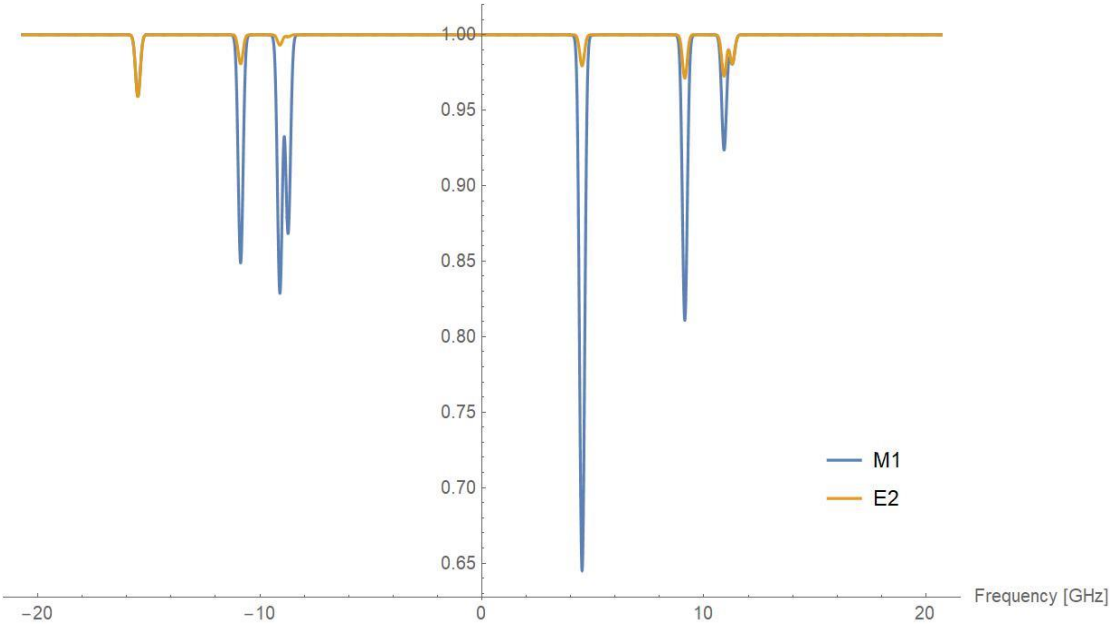


*Figure 10: Calculated transmission spectrum of the $5^2P_{3/2} \rightarrow 5^2P_{1/2}$ M1 and E2 transition of atomic $^{127}I$, calculated separately for each multipole transition's contribution.*

The combined transmission for the M1 and E2 transitions is depicted in the figure below.

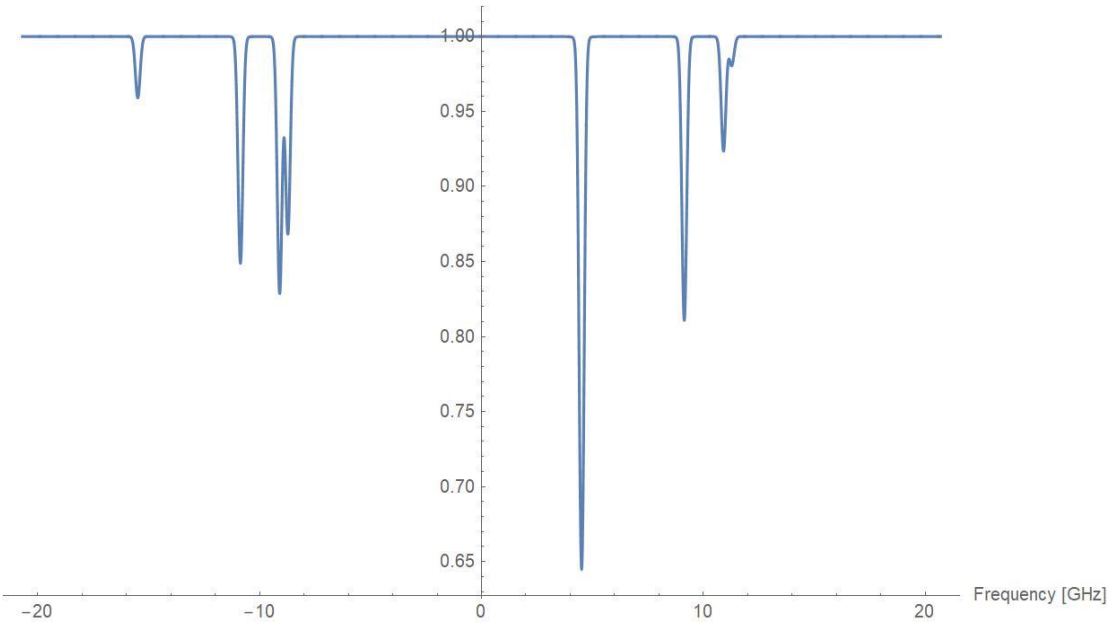


*Figure 11: Calculated transmission spectrum of the $5^2P_{3/2} \rightarrow 5^2P_{1/2}$ M1 and E2 transition of atomic $^{127}I$ (total contribution).*

## Photodissociation of $I_2$ [3]

The method used to create the ground state $^2P_{3/2}$ of atomic iodine was the photodissociation of molecular iodine $I_2$ (assumed to be in the ground molecular state) with a green 532nm laser (at low pressure, in room temperature) and is presented in [3]. The photodissociation reaction is written in the equation below

$$I_2 + h\nu \rightarrow I + I \tag{71}$$

where $I \equiv I(2P_{3/2})$. After the creation of atomic iodine, it is recombined to its molecular state through two main processes that are:

- Three-body recombination: $I + I + I_2 \rightarrow 2I_2$
- Sticking on the container walls: $\begin{cases} I + wall \rightarrow I_{wall} \\ I_{wall} + I_{wall} \rightarrow I_2 \end{cases}$ (72)

We note that the three-body recombination reaction can also occur in the presence of another third body other than $I_2$, but the $I_2$ channel is the most effective (i.e., it has the higher rate). These two processes can be characterized by the rate at which they produce molecular iodine, that is $k_r$ for the first process, and $k_w$ for the second.

We can write the rate of the atomic iodine production in the equation below:

$$\frac{d[I]}{dt} = \sigma\Phi[I_2] - k_r[I]^2[I_2] - k_w[I] \tag{73}$$

where $[I]$ and $[I_2]$ stand for atomic and molecular iodine densities, respectively, $\sigma = 2.4 \times 10^{-18} cm^2$ is the $I_2$ photodissociation cross section at 532nm, and the green laser photon flux is

$$\Phi = \frac{1}{A}\frac{P}{hc/\lambda} \tag{74}$$

where $P$ is the power of green laser, with $A$ the cell cross sectional area.

By solving the differential *Equation (73),* we get the steady state solution

$$[I]_\infty = \frac{-k_w + \sqrt{k_w^2 + 4[I_2]^2 k_r \sigma\Phi}}{2[I_2]k_r} \tag{75}$$

In the experiment we used a high-power photo-dissociating green laser, and an uncoated iodine glass cell, which we heated to around 50° C, as described in more detail in the experimental section of this thesis. The combination yielded high atomic iodine, steady-state densities, enough to make the M1 transition optically thick at the most pronounced resonances (> 10 optical depths), in a tunable way (by tweaking the green laser power and the temperature of the cell). These optical thicknesses were necessary to be able to observe the very weak E2 contribution to the transition.

## Dominant line-broadening mechanisms

### Gaussian profile

The gaussian profile is a result of the Doppler broadening, as the velocity of the atoms (or molecules) relative to the observer follows a Maxwell distribution, which is temperature dependent. The gaussian profile satisfies the formula

$$g(v) = h_D + \frac{A_D}{\Delta f_D \sqrt{\pi}} \exp\left[-\left(\frac{v - v_0}{\Delta f_D}\right)^2\right] \quad (76)$$

where $v$ is the frequency variable, $h_D$ is the vertical shift of the distribution, $\frac{A_D}{\Delta f_D \sqrt{\pi}}$ is the maximum value of the distribution at the central frequency $v_0$, and $\Delta f_D$ is the half width at $1/e$ of the maximum value (HW@1/eM), that satisfies the relation $\Delta\omega_D = 2\pi \cdot \Delta f_D$. This parameter is related with the full width at half maximum (FWHM) through the relation

$$(FWHM)_{Gaussian} = \Delta f_D 2\sqrt{\ln(2)} \quad (77a)$$

with its error

$$\delta(FWHM)_{Gaussian} = \delta(\Delta f_D)\, 2\sqrt{\ln(2)} \quad (77b)$$

## Voigt profile

The Voigt profile is a convolution of a Lorentzian and a Gaussian distribution. The Lorentzian distribution is a result of the lifetime broadening (uncertainty in energy), while the Gaussian is due to the Doppler broadening, as mentioned previously.

The formula of the Voigt profile we used is defined through a function called the Faddeeva function or Kramp function. The Voigt profile satisfies the formula

$$V = V_0 + A\frac{Re[w]}{\sigma\sqrt{2\pi}} \quad (78a)$$

where $V_0$ is the vertical shift of the distribution, $A$ is a constant that determines the high of the distribution, and the rest variables are defined below. The Faddeeva function is

$$w = \exp(-z^2) * erfc(-iz) \quad (78b)$$

with

$$z = \frac{v - v_0 + i\gamma}{\sigma\sqrt{2}} \quad (78c)$$

where $i = \sqrt{-1}$ is the imaginary number, $\gamma$ is the half width at half maximum (HWHM) of a Lorentzian distribution, $\sigma$ is the standard deviation of the Gaussian profile related to its HWHM, $a$, by

$$a = \sigma\sqrt{2\ln(2)} \quad (78d)$$

and $erfc(x)$ is the error function that is defined as

$$erfc(x) = \frac{2}{\sqrt{\pi}}\int_0^x e^{-t^2} dt \quad (78e)$$

The $FWHM$ of the Voigt profile is estimated approximately by the relation (from [8] as mentioned in [2])

$$(FWHM)_{Voigt} \approx \frac{f_L}{2} + \sqrt{\frac{f_L^2}{4} + f_G^2} \quad (79a)$$

with its error

$$\delta(FWHM)_{Voigt} \approx \sqrt{\left(\left(\frac{1}{2}+\frac{f_L}{4\sqrt{\frac{f_L^2}{4}+f_G^2}}\right)\delta f_L\right)^2+\left(\frac{f_G}{\sqrt{\frac{f_L^2}{4}+f_G^2}}\delta f_G\right)^2} \quad (79b)$$

with

$$f_L = 2\gamma$$
$$f_G = 2\sigma\sqrt{2ln2} \quad (79c)$$

where $f_L$ and $f_G$ are the Lorentzian and Gaussian FWHMs, respectively, defined with respect to the variables $\gamma$ and $\sigma$ from the Voigt formula.

## Experimental scheme

The experimental setup is shown in *Figure* 12 and a photo of the cavity configuration is shown in *Figure 13*. The setup comprised of a bowtie cavity with length $L = 2.6\text{m}$, and $FSR = 115\text{MHz}$**.** The empty-cavity Finesse was $\mathcal{F} \simeq 240$. This type of resonator consists of four highly reflective mirrors; here, two of them were curved with radius of curvature of 2m and nominal reflectivities of 99.99% and 99.5% (output coupler), and the other two were plane with reflectivity of 99.99% and 99.5% (input coupler). A green continuous wave (cw) laser at 532nm was used for the dissociation of iodine $I_2$ molecules to $2 \times I$. We used a chopper to periodically chop the photo-dissociating beam. The IR laser at 1315nm was used to probe the atomic M1 and E2 transition lines. The IR laser was the tunable diode laser DL pro from Toptica Photonics and we operated it from its driver circuit that is composed of some independent modules (i.e., the analog interface, DigiLock 110, the feedback controller used to lock the laser frequency to cavity resonances, SC 110 the scan controller, DTC 110 the temperature controller, DCC 110 the current controller, DC 110 the diode laser controller).

The iodine cell was 45 cm in length, and 8 mm in diameter (internal), and two highly AR-coated windows were glued with epoxy glue at its edges. The windows were AR-coated for both 1315 nm and 532 nm (from EKSMA). The cell was wrapped with heat tapes across its whole length, except for the iodine holder part (there was a valve separating this compartment from the cell's interior). In this way, the heat tapes could maintain a cell temperature of ~100°C, but the iodine vapor pressure was determined by the iodine holder cold spot, the temperature of which was individually controlled, and was kept at ~50°C. Heating the cell in this way also prevented iodine from being deposited on the cell windows, which would lead to compromised AR performance and reduced cavity finesse.

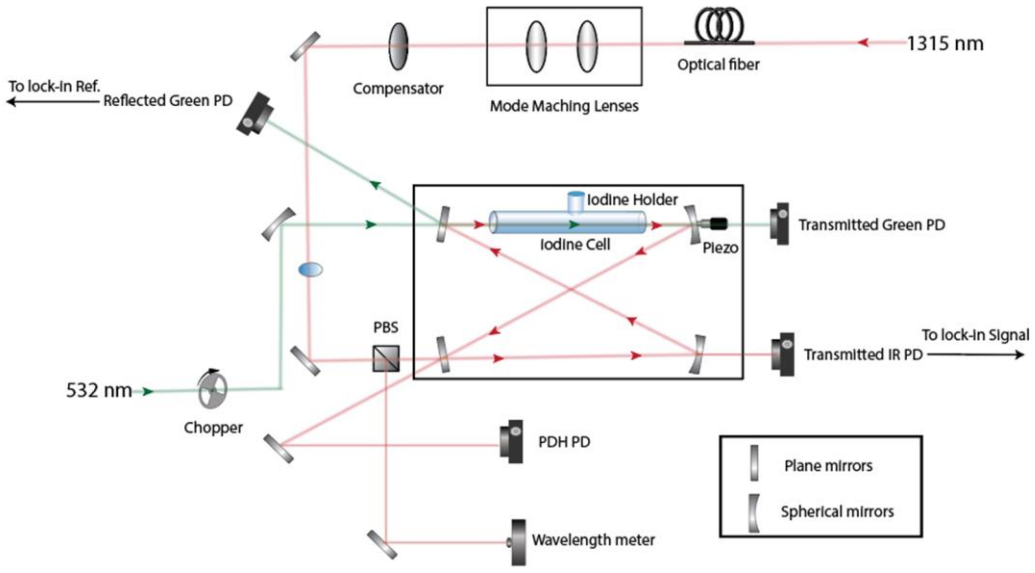


*Figure 12: Schematic diagram of the experimental setup. Image from Toutoudaki - Master Thesis [4]*

Experimental scheme,

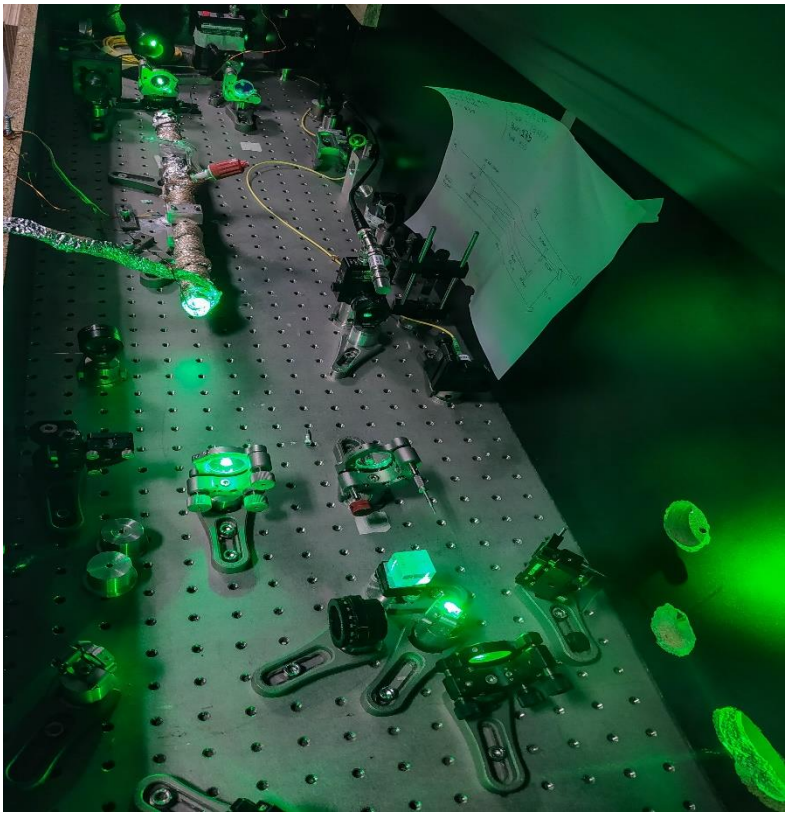

*Figure 13: Photo of the cavity configuration*

## Experiment

We locked the IR laser on a specific frequency of the cavity's resonances (on a specific mode) with the *Pound-Drever-Hall (PDH) technique* [14]. Then we used a piezoelectric transducer on which a cavity mirror was mounted, in order to control the cavity length on a micrometer scale. By modifying the cavity's length, we changed the frequencies at which the cavity resonates and as the laser remained locked on a mode we were able to follow the "movement" of this mode in the frequency domain with the laser. We measured the laser wavelength with a wavelength meter (Bristol 671), and this value, along with the value of the wavelength we wanted to reach, was the input at the program *LabVIEW PID*. This program calculated the difference of these two values and -through a device that converted the wavelength difference to voltage signals- was sending feedback to the piezoelectric transducer of the cavity's mirror that stabilized the frequency further. In this way, we were able to control the laser's exact frequency and scan over the iodine resonances.

We had the green laser operated with a current of $30\mathrm{A}$, that corresponds to power of $50\mathrm{W}$ approximately. The heat tapes were heated at $100°\mathrm{C}$ and the cold spot was around $50°\mathrm{C}$. By heating the iodine cell, we increased the vapor pressure of the iodine, resulting in higher molecular iodine densities. By operating on these conditions, we took measurements of the transmission signal for different wavelengths in the region of M1 and E2 transitions. The data acquired by the oscilloscope (that permitted averaging) for a specific wavelength (here for $1315.3280\ \mathrm{nm}$) are plotted in *Figure 14*.

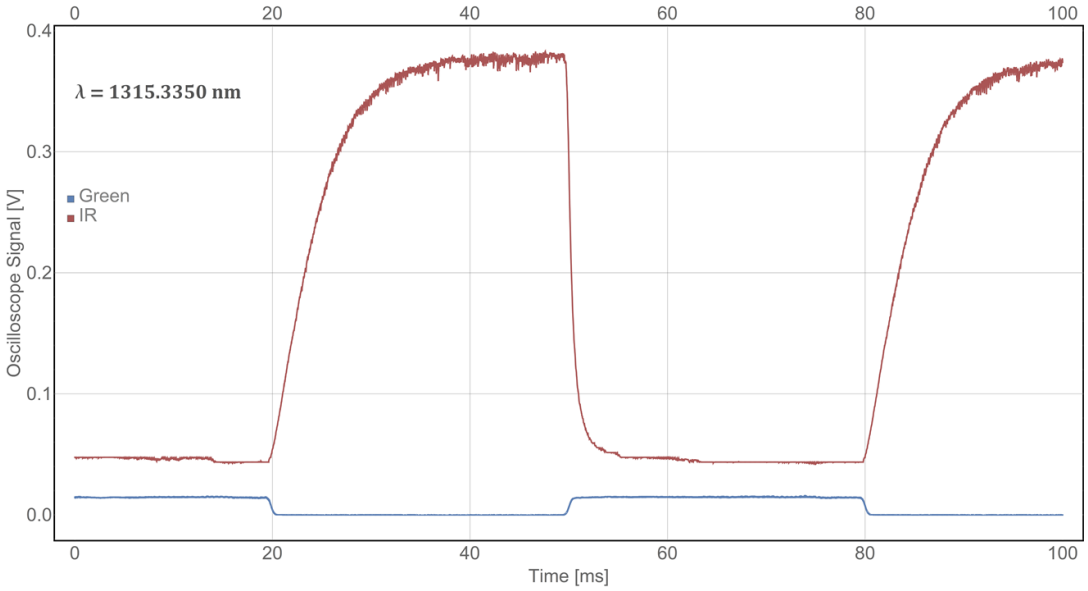


*Figure 14: Measured power of the green and IR laser at 1315.3280 nm*

There were two signals from the photodiodes; one from the green laser reflected off the cavity that was periodically chopped, and the other from the IR laser transmitted through the cavity. The beams overlaid with each other and both interacted with the iodine; the green beam photodissociated the molecular iodine and was producing its atomic form, and the IR beam was absorbed by the atomic iodine in order to study its transitions. So, as we see in *Figure 14*, the change of intensity of the IR signal reflects the periodicity of the green beam's intensity modulation. We observe that when the green beam was on (meaning that it passed through the chopper, photodissociated the molecular iodine, and produced atomic iodine) the IR beam's output had less intensity than when the green beam was off (meaning that it was

blocked by the chopper, and atomic iodine was not produced). Therefore, the green beam had to be on, in order to create atomic iodine, that in turn absorbs the IR beam.

For each wavelength measured, we calculated the normalized transmission of the IR laser after interacting with the iodine as the ratio of the mean values of the IR power when the green beam was on divided by the mean values of the IR power when the green beam was off. The plot of the transmission coefficient with respect to the wavelengths measured is presented in *Figure 15*.

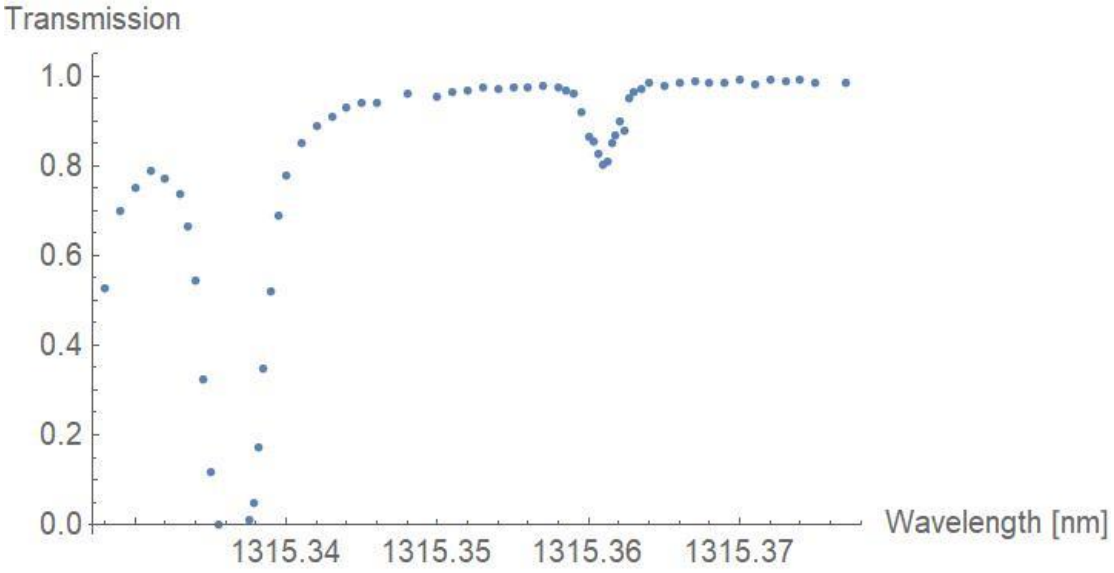


*Figure 15: Plot of the transmission coefficient of the IR radiation versus the wavelength*

On the previous figure, the deepest trough (to the left) of the transmission coefficient represents the $3 \rightarrow 2$ M1 transition and the shallower one (to the right) the $4 \rightarrow 2$ E2 transition. By converting the wavelength axis to frequency, and the transmission coefficient to absorption coefficient through the Beer Lambert law, we get the following diagram, in *Figure* 16, with the same information as the previous, in *Figure 15*, from different perspective. In the horizontal axis we have estimated the frequency shift (or detuning) from a central frequency.

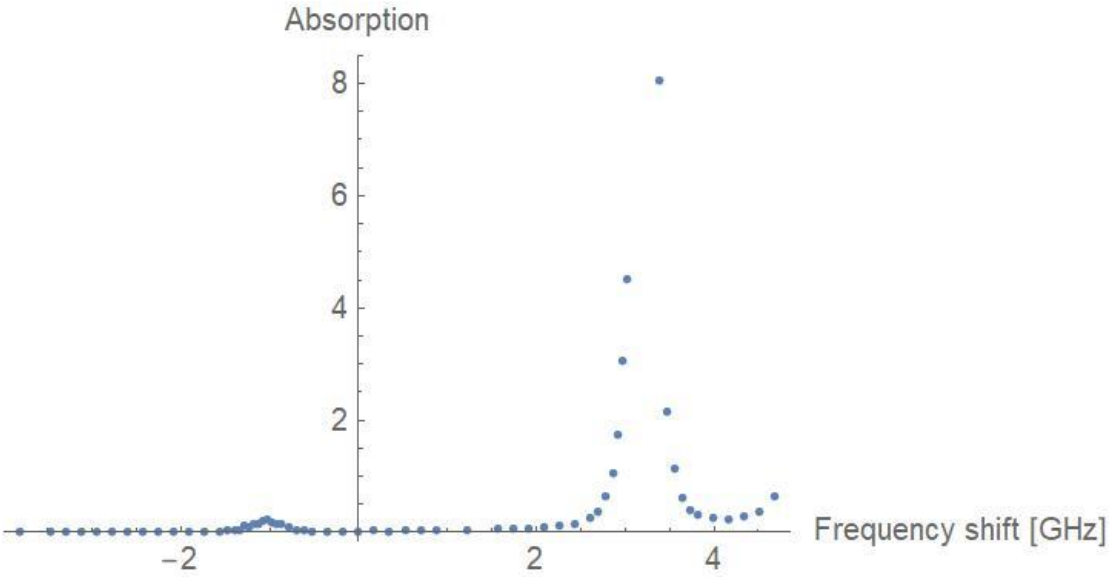


*Figure 16: Plot of the absorption coefficient of the IR radiation versus the frequency detuning*

## Fitting on the spectrum lines

In this section, we fitted on each transition separately a gaussian and a Voigt profile. After that, we tried to compile the previous fitted functions in one to fit on both of the transitions, simultaneously. From these fits, we extracted the characteristics of the absorption curves, and specifically the width of the transitions.

### M1 transition

Firstly, we studied the $3 \rightarrow 2$ M1 transition, where we adapted a gaussian profile that is demonstrated in the figure below.

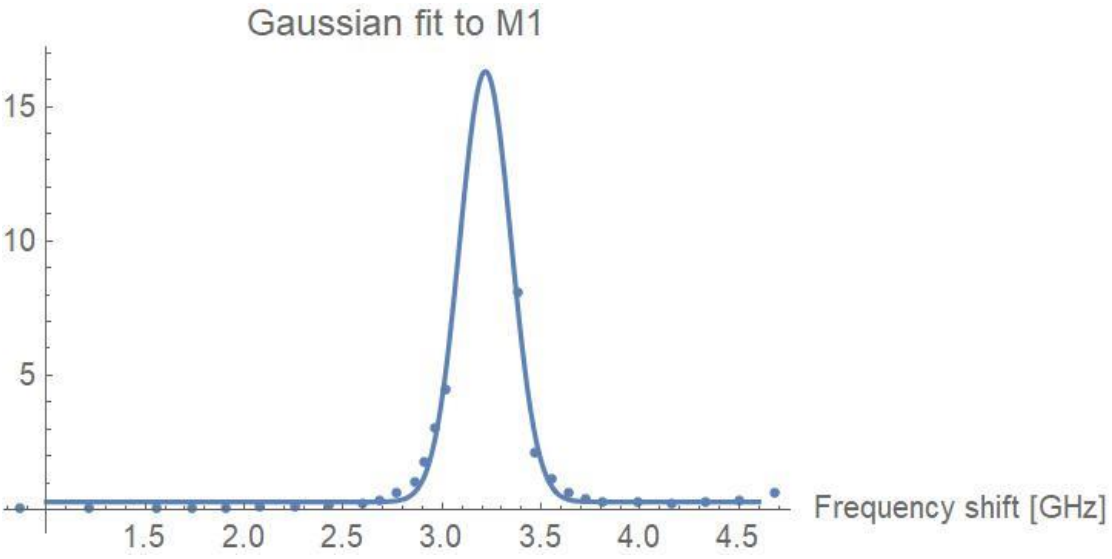


*Figure 17: Gaussian fit to M1 line*

The Gaussian parameters of this fit are presented in the table below.

| Gaussian parameters of M1 fit |
|---|
| $\Delta f_D = (184 \pm 8) MHz$ |
| $v_0 = (3.218 \pm 0.004) GHz$ |
| $h_D = (0.29 \pm 0.07)$ |
| $A_D = (5.2 \pm 0.3)$ |

The value of $v_0$ value is measured in terms of the frequency detuning from the central frequency of the plot.

The $R^2$ value of the fit was $97.50\%$ and the $(\boldsymbol{FWHM})_{\boldsymbol{Gaussian,M1}} = (\boldsymbol{306 \pm 14})\ \boldsymbol{MHz}$.

Then, we fitted a Voigt profile on this spectral line, and we got the fit plotted in the figure below.

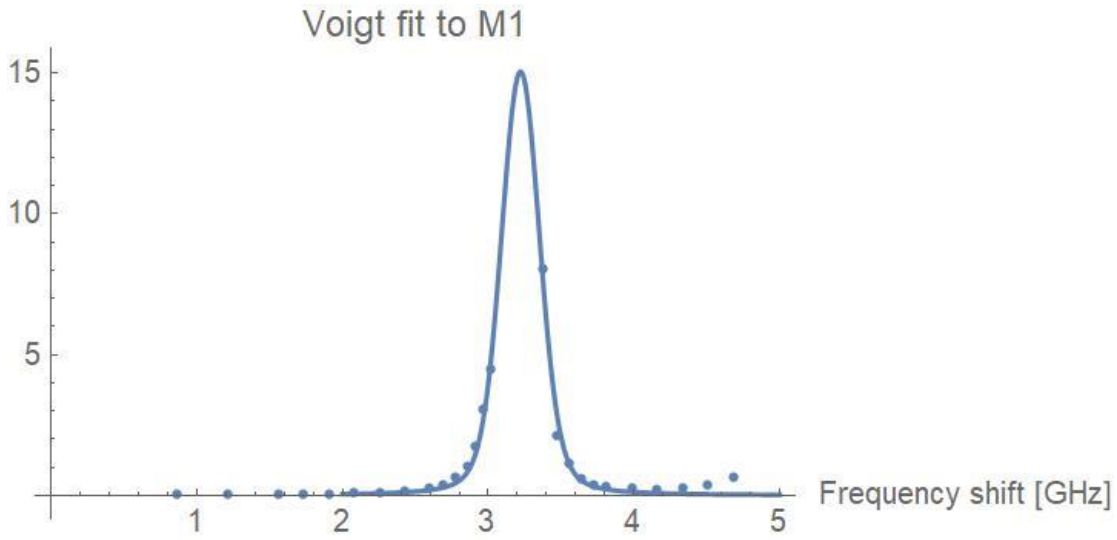


*Figure 18: Voigt fit to M1 line*

The parameters of the Voigt profile here were:

| Voigt parameters of M1 fit |
|---|
| $\gamma = (38 \pm 10) MHz$ |
| $\sigma = (114 \pm 6) MHz$ |
| $v_0 = (3.221 \pm 0.003)$GHz |

the $R^2$ value was $97.62\%$, and the $(\boldsymbol{FWHM})_{\boldsymbol{Voigt,M1}} = (\boldsymbol{310 \pm 19})\ \boldsymbol{MHz}$.

## E2 transition

About the $4 \rightarrow 2$ E2 transition, we fitted a gaussian profile plotted below, with its parameters on the table that follows.

Experiment, Fitting on the spectrum lines

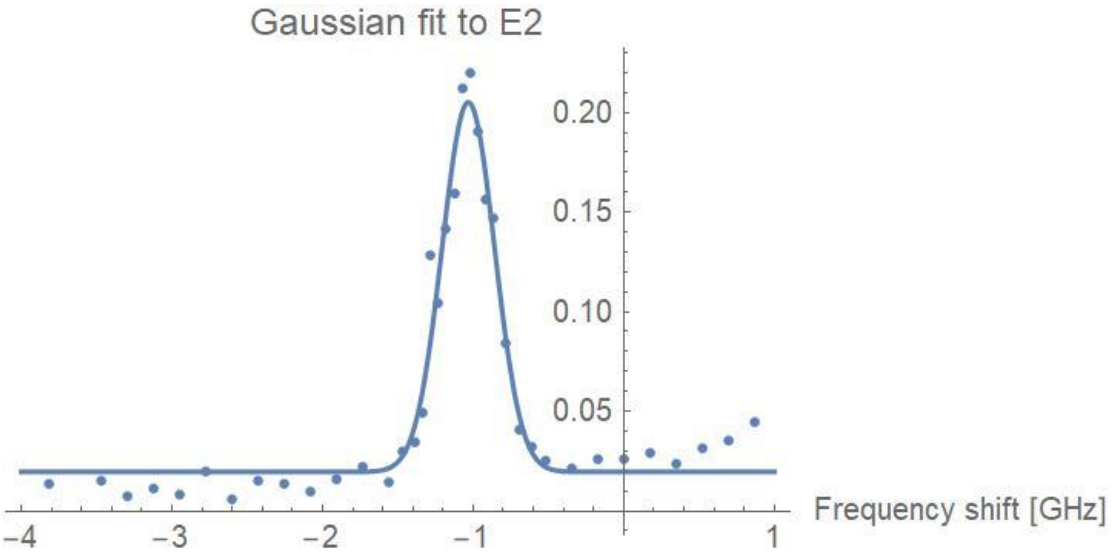


*Figure 19: Gaussian fit to E2 line*

| Gaussian parameters of E2 fit |
|---|
| $\Delta f_D = (247 \pm 12) MHz$ |
| $v_0 = (-1.032 \pm 0.008) GHz$ |
| $h_D = (0.020 \pm 0.003)$ |
| $A_D = (0.081 \pm 0.004)$ |

The $R^2$ value was 97.70%, and the $(\boldsymbol{FWHM})_{\boldsymbol{Gaussian,E2}} = (\boldsymbol{411 \pm 20})\ \boldsymbol{MHz}$.

And then, we adapted a Voigt profile on the E2 spectrum line with its graph and parameters presented below.

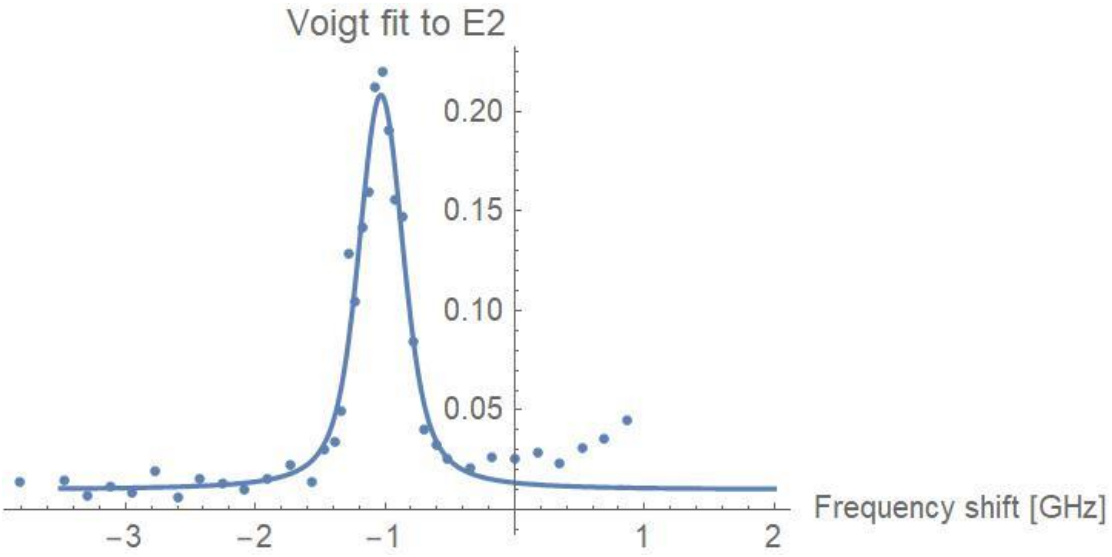


*Figure 20: Voigt fit to E2 line*

| Voigt parameters of E2 fit |
|---|
| $\gamma = (108 \pm 43) MHz$ |
| $\sigma = (118 \pm 35) MHz$ |
| $v_0 = (-1.031 \pm 0.008)$GHz |

The $R^2$ value of the fit was $97.30\%$ and the $(\boldsymbol{FWHM})_{\boldsymbol{Voigt,M1}} = (\boldsymbol{406 \pm 97})\ \boldsymbol{MHz}$.

## M1 & E2 transitions

Eventually, we compiled two Voigt profiles to fit both peaks and the result is shown in the two next figures.

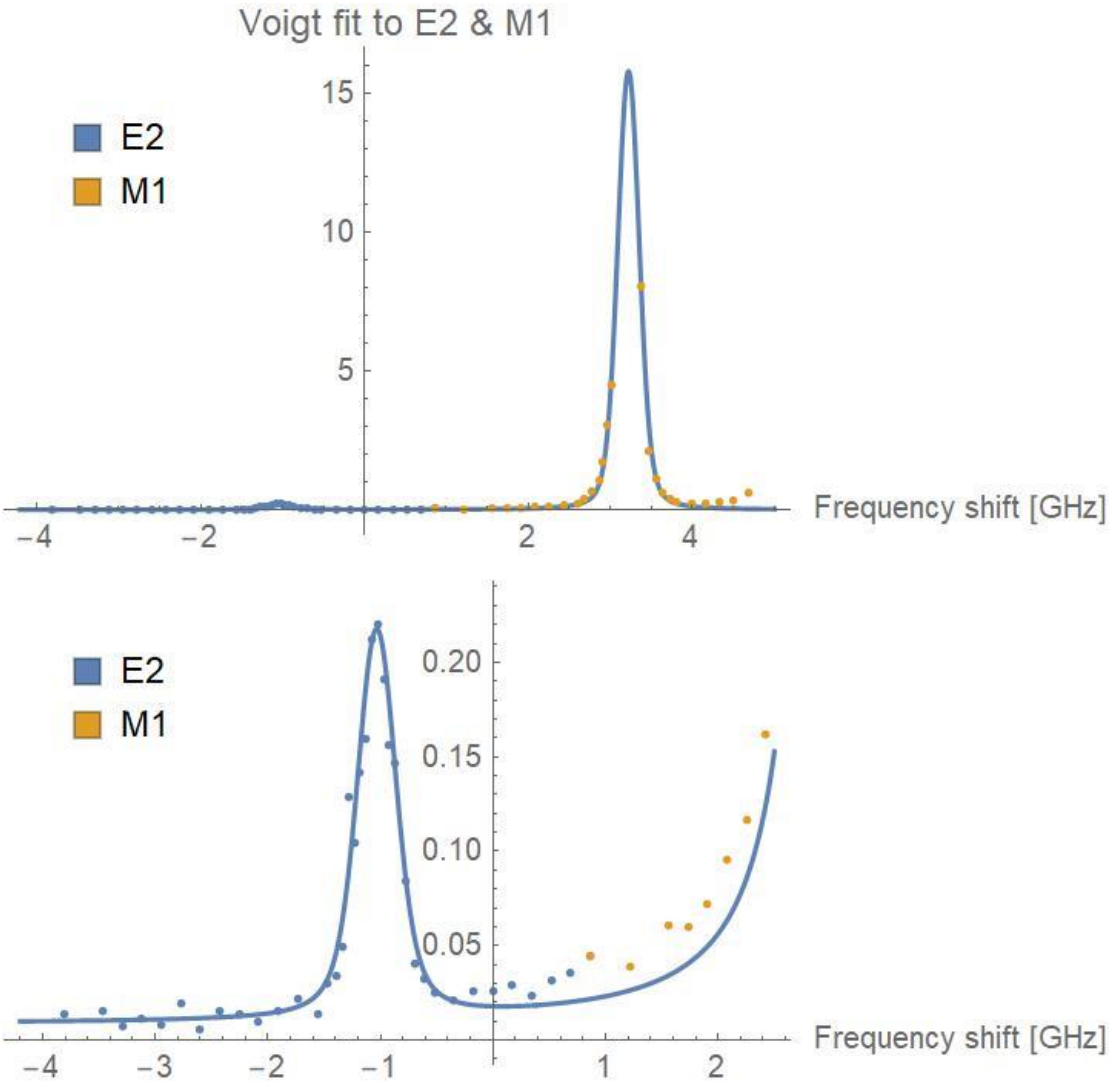


*Figure 21: Voigt fit to M1 and E2 lines*

The $R^2$ value of the fit was $97.91\%$.

The electric quadrupole to magnetic dipole ratio parameter, $\chi$, can be extracted from the following relation:

$$\chi = \sqrt{\frac{(2F_1+1)(2F_1'+1)}{(2F_2+1)(2F_2'+1)}} \frac{\begin{Bmatrix} J & 1 & J' \\ F_1' & I & F_1 \end{Bmatrix}}{\begin{Bmatrix} J & 2 & J' \\ F_2' & I & F_2 \end{Bmatrix}} \sqrt{r} \tag{80}$$

where $r$ is the ratio of the peaks of $E2$ to $M1$, the parameters $\boldsymbol{F_2 = 4 \rightarrow F_2' = 2}$ are related to the $E2$ transition, while $\boldsymbol{F_1 = 3 \rightarrow F_1' = 2}$ to the $M1$ transition, and $J = 3/2, J' = 1/2, I = 5/2$ are the total electronic angular momentum of the ground state, the initial state, and the spin angular momentum of the nucleus, respectively.

The experimental ratio of the E2 to M1 heights was calculated to be: $r = \frac{h_{E2}}{h_{M1}} = \frac{0.22}{15.6} = 0.014 \pm 0.001$.

So, the value we calculated for the $\chi$ parameter is $\boldsymbol{\chi \approx 0.085 \pm 0.004}$, that has around $4.5\%$ difference with preliminary theoretical calculations that yield the value $\chi_{th} = 0.081$ by V. A. Dzuba, UNSW.

## Conclusion

In conclusion, we successfully measured the E2 component of the atomic iodine transition and we estimated the ratio of the reduced matrix elements of the electric-quadrupole to magnetic-dipole transition, the parameter $\chi$.

Possible improvements, that could help further on this direction in future measurements, are to use a cavity with better finesse and a longer cell. These changes would increase the effective pathlength of the light in the cavity. So, the light would interact for longer distance with the absorber, resulting in greater absorption of the IR light beam. Also, better manipulation of the green beam and more accurate temperature control would optimize the obtained atomic iodine densities, giving an optically thicker transition. In these ways, we can obtain greater absorption signals, enhancing the weak E2 transition we are interested in, and make more precise measurements of the $\chi$ parameter.

# Acknowledgments

First of all, I would like to thank my supervisor Prof. T. Peter Rakitzis who gave me the opportunity to participate in his lab. Through my participation I had a great chance to learn such a lot of things and to meet great people working and studying there.

Then, I would like to thank George Katsoprinakis and Eirini Toutoudaki who were very helpful and patient along this work. We spent hours together in order to get familiar with the theory and the experiment while we were working on the project. Without them it would not be possible to complete this thesis, and I am glad I met them and we worked together for this time period.

Also, I want to thank Kostas Tazes, who, along with Mr. Katsoprinakis, spent time with me correcting the writing of the thesis and suggesting appropriate changings. Their suggestions were important to me and I am grateful for their support. Also, another person who I appreciated his help is Alexandros Zarafonitis, who helped me to clarify some aspects of this thesis' theory.

I would like to thank the rest of the members of this lab; Michalis Xygkis, Michalis Koutrakis and Artemis Linaraki for creating this cooperative environment that was pleasant to work there.

And, finally, I would like to thank my family and friends for their support and encouragement.

# References

[1] Verdeyen, J. T. (1995). *Laser electronics*. Prentice Hall

[2] Olivero, J. J.; R. L. Longbothum (February 1977). "Empirical fits to the Voigt line width: A brief review". Journal of Quantitative Spectroscopy and Radiative Transfer. 17 (2): 233–236. Bibcode:1977JQSRT..17..233O. https://doi.org/10.1016/0022-4073(77)90161-3. ISSN 0022-4073.

[3] Katsoprinakis, G., Chatzidrosos, G., Kypriotakis, J. et al. High steady-state column density of I(2P3/2) atoms from I2 photodissociation at 532 nm: Towards parity non-conservation measurements. Sci Rep 6, 33261 (2016). https://doi.org/10.1038/srep33261

[4] Toutoudaki, E. (2021). Cavity-enhanced atomic Iodine spectroscopy: Towards PNC optical rotation measurements [Master Thesis]. University of Crete.

[5] Fitzpatrick, R. (2015) *Quantum Mechanics*, World Scientific. https://doi.org/10.1142/9789814689991_0008.

[6] Brederlow, G., Fill, E., Witte, K. J. (1983). *The high-power iodine laser*. Springer-Verlag Berlin

[7] Bougas, L., Katsoprinakis, G. E., von Klitzing, W. & Rakitzis, T. P. “Fundamentals of cavity-enhanced polarimetry for parity-nonconserving optical rotation measurements: Application to Xe, Hg, and I”. Phys. Rev. A 89, 052127, 10.1103/PhysRevA.89.052127 (2014).

[8] Van De Hulst, H. C., Reesinck, J. J. M. (1947). “Line Breadths and Voigt Profiles”. Astrophys. J. 106, 121. DOI: 10.1086/144944.

[9] Deng, L. hua, Li, X. yun, Zhu, Y. yue & Chen, Y. qin. (2015). ‘Hyperfine structure near infrared spectrum of atomic iodine’. J. Quant. Spectrosc. Radiat. Transf. 161, 153–156 https://doi.org/10.1016/j.jqsrt.2015.04.012

[10] Katsoprinakis, G. E., Bougas, L., Rakitzis, T. P., Dzuba, V. & Flambaum, V. V. “Calculation of parity-nonconserving optical rotation in iodine at 1315 nm”. Phys. Rev. A 87, 040101(R), 10.1103/PhysRevA.87.040101 (2013).

[11] Bougas, L., Katsoprinakis, G. E., von Klitzing, W., Sapirstein, J. & Rakitzis, T. P. “Cavity-Enhanced Parity-Nonconserving Optical Rotation in Metastable Xe and Hg”. Phys. Rev. Lett. 108, 210801, 10.1103/PhysRevLett.108.210801 (2012).

[12] Department of Physics and Astronomy, Georgia State University. (2016). *HyperPhysics*. Quantum Physics. http://hyperphysics.phy-astr.gsu.edu/hbase/quacon.html#quacon. http://hyperphysics.phy-astr.gsu.edu/hbase/Atomic/lcoup.html.

[13] Foot, C. J. (2005). *Atomic Physics*. Oxford University Press

[14] Black, E. (1998). *Notes on the Pound-Drever-Hall technique* [Internal working note of the LIGO Project]. California Institute of Technology, Massachusetts Institute of Technology. https://dcc.ligo.org/public/0028/T980045/000/T980045-00.pdf.